Evolution of Multiscale Vortices in the Development of Hurricane Dolly (2008)

JUAN FANG

Key Laboratory of Mesoscale Severe Weather (MOE), Department of Atmospheric Sciences, Nanjing University, Nanjing, China

FUQING ZHANG

Department of Meteorology, The Pennsylvania State University, University Park, Pennsylvania

(Manuscript received 6 April 2010, in final form 6 July 2010)

ABSTRACT

As a follow-up to a previously published article on the initial development and genesis of Hurricane Dolly (2008), this study further examines the evolution of, and interactions among, multiscale vortices ranging from the system-scale main vortex ($L > 150$ km) to the intermediate-scale cloud clusters (50 km $< L <$ 150 km) and individual vorticity-rich convective cells ($L < 50$ km). It is found that there are apparent self-similarities among these vortices at different scales, each of which may undergo several cycles of alternating accumulation and release of convective available potential energy. Enhanced surface fluxes below individual cyclonic vortices at each scale contribute to the sustainment and reinvigoration of moist convection that in turn contributes to the maintenance and upscale growth of these vortices.

Spectral analysis of horizontal divergence and relative vorticity further suggests that the cloud-cluster-scale and system-scale vortices are predominantly balanced while the individual convective vortices are largely unbalanced. The vorticity and energy produced by these individual vorticity-rich convective cells first saturate at convective scales that are subsequently transferred to larger scales. The sum of the diabatic heating released from these convective cells may be regarded as a persistent forcing on the quasi-balanced system-scale vortex. The secondary circulation induced by such forcing converges the cluster- and convective-scale vorticity anomalies into the storm center region. Convergence and projections of the smaller-scale vorticity to the larger scales eventually produce the spinup of the system-scale vortex. Meanwhile, convectively induced negative vorticity anomalies also converge toward the storm center, which are weaker and shorter lived, and thus are absorbed rather than expelled.

1. Introduction

Along with advances in remote observations and numerical simulations, more and more small-scale (several to a few tens of kilometers) features and processes associated with tropical cyclones (TCs) have been identified. Marks and Houze (1984) were the first to identify small-scale vortices in the eyewall of a TC using airborne Doppler radar data. It was found that the small-scale vortices were associated with the maximum values of convergence, vorticity, and wind speed in the TC, suggesting that they played significant roles in the storm's dynamics. Marks et al. (2008) presented a detailed observational view of a vortex in the eyewall of Hurricane Hugo (1989). The analysis revealed that the intense cyclonic vorticity maximum adjacent to the strongest convection in the eyewall was roughly 1 km in diameter with a magnitude of 1.25×10^{-1} s^{-1}. Also using Doppler radar data, Reasor et al. (2005) and Sippel et al. (2006) provided observational evidence for the existence and interactions of intense vortices associated with individual cumulonimbus clouds of varying scales and intensities in developing cyclones.

With aid from high-resolution convection-permitting simulations of TCs, the small-scale processes and their subsequent roles in the development and evolution of TCs have been explored in greater detail. Hendricks et al. (2004) suggested that convective plumes with intense vertical vorticity in their cores, that is, vortical hot towers (VHTs), are the preferred convective structures in tropical cyclogenesis. Such features can precondition

Corresponding author address: Dr. Juan Fang, Key Laboratory of Mesoscale Severe Weather (MOE), Dept. of Atmospheric Sciences, Nanjing University, Nanjing 210093, China.
E-mail: fangjuan@nju.edu.cn

DOI: 10.1175/2010JAS3522.1

the local environment via diabatic production of multiple small-scale lower-tropospheric cyclonic potential vorticity (PV) anomalies and, eventually, result in the spinup of TCs through multiple mergers and axisymmetrization of these low-level PV anomalies. Montgomery et al. (2006) further demonstrated that the VHTs can effectively overcome the generally adverse effects of downdrafts and be sustained for a relatively long time period by consuming convective available potential energy (CAPE) in their local environment, humidifying the middle and upper troposphere, and undergoing diabatic vortex mergers with neighboring towers. Both Hendricks et al. (2004) and Montgomery et al. (2006) argued that the VHTs collectively mimic a quasi-steady diabatic heating forcing within the cyclonic environment and are responsible for the development of a quasi-balanced secondary circulation on the system scale, which converges the environmental cyclonic vorticity and VHTs, and induces the spinup of the vortex on the system scale. Despite using a lower-resolution model, Tory et al. (2006a,b) also found the formation and merger of VHT-like anomalies resulted in the formation of a dominant vortex that became the TC core in simulations of tropical cyclogenesis in Australia. All of the aforementioned numerical studies suggest a new paradigm on TC genesis, which occurs within a vorticity-rich environment via VHTs and their aggregate effects. It is argued that the existence of sufficient CAPE and low-level cyclonic vorticity in pre-TC environments facilitates the formation of VHTs by deep convective processes, which serve as the primary building blocks of the TC vortex. There is some observational evidence suggesting such a VHT path to tropical cyclogenesis and TC development. For example, with Doppler radar data from Hurricane Dolly (1996), Reasor et al. (2005) found that the low-level vortex enhancement on the convective scale is consistent with the VHT theory. The intense vortices associated with individual cumulonimbus clouds identified by Sippel et al. (2006) through radar data from Tropical Storm Allison (2001) exhibited vortex interactions similar to those discussed in Hendricks et al. (2004) and Montgomery et al. (2006).

The small-scale vortices, such as VHTs, and their aggregate effects are also argued to play a prominent role in the rapid intensification of TCs. Earlier investigators suggested that the cooperative interaction between deep convection and the surface large-scale circulation is a positive feedback process, by which an incipient tropical disturbance can be intensified and ultimately developed into a TC; this positive feedback process was coined conditional instability of the second kind (CISK; Charney and Eliassen 1964; Ooyama 1964). Since the late 1980s, the CISK mechanism has been challenged by the wind-induced surface heat exchange instability (WISHE), a principal theory proposed as an alternative to CISK by Emanuel (1986) and Rotunno and Emanuel (1987). Within the WISHE framework, a positive feedback between the azimuthal-mean boundary layer equivalent potential temperature and the azimuthal-mean surface wind speed underneath the eyewall of the storm fuels the intensification of the TC vortex. Recently, Nguyen et al. (2008) suggested that VHTs are able to extract surface moisture fluxes that are locally sufficient for growth without the wind–moisture feedback that typifies WISHE, and therefore the WISHE feedback mechanism is much less of a constraint on the development of TCs in three dimensions. Montgomery et al. (2009) further argued that the TC intensification in three dimensions is dominated by VHTs while the evaporation–wind feedback process is not essential.

With the development of VHTs induced by convection, remarkable negative vorticity anomalies are also produced through tilting and stretching effects, as is also the case in Davis and Bosart (2006). The evolution of such negative vorticity anomalies in the development of TCs is another interesting issue associated with small-scale vortices. Through idealized numerical experiments based on a 3D quasigeostrophic model, Montgomery and Enagonio (1998) showed that vortex intensification was preceded by the ingestion of like-signed PV anomalies into the parent vortex and expulsion of opposite-signed PV anomalies during the axisymmetrization process. With a shallow water model, Nolan et al. (2001) demonstrated that the low-vorticity core moves radially outward toward the outer edge of the eyewall, where it is then sheared apart by the large angular velocity gradients that exist in that region of the vortex. Based on idealized TC simulations with a full-physics primitive-equation 3D model, Nguyen et al. (2008) also argued that cyclonic vorticity anomalies in the negative vorticity gradient of the parent vortex will tend to move toward the center, while anticyclonic anomalies will tend to move away from the center. Although the above-mentioned studies suggest the expulsion of the negative vortices, the role of the low-level convergent flow on the evolution of negative vortices goes unmentioned.

The current study seeks to understand the dynamics and thermodynamics that govern the patterns of evolution and impacts of convectively induced vortices at different scales via a cloud-resolving simulation (highest horizontal resolution is 1.5 km) of Hurricane Dolly (2008) with the Weather Research and Forecasting model (WRF) (Fang and Zhang 2010, hereafter referred to as FZ10). It is demonstrated in FZ10 that the model reproduces reasonably well the track and intensity as compared to available observations. Thus, the simulation provides a four-dimensional, dynamically consistent, high-resolution dataset useful for gaining insights into the evolution of small-scale vortices during the formation of Dolly.

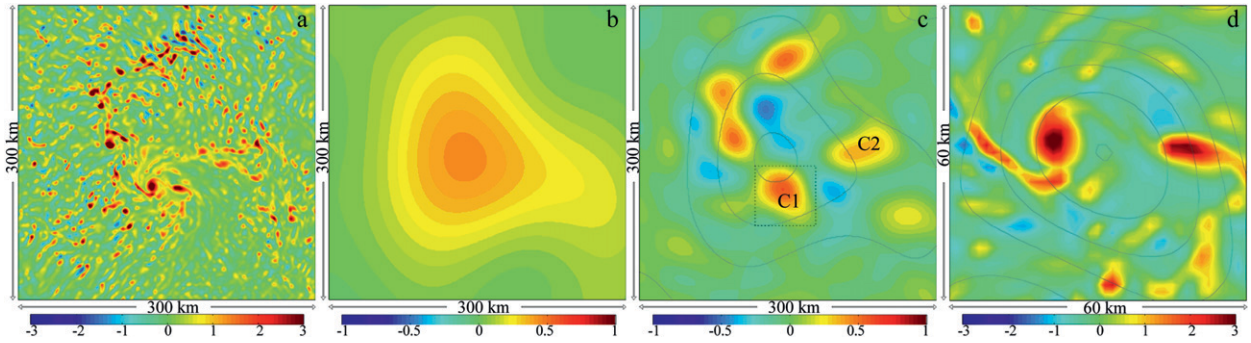

FIG. 1. (a) Horizontal distribution of the 188-m relative vorticity (shaded, 0.5×10^{-3} s^{-1}) valid at 0300 UTC 22 Jul 2008. (b)–(d) As in (a), but for scales (b) greater than 150 km, (c) between 50 and 150 km, and (d) smaller than 50 km. Panels (a)–(c) are plotted in the storm-centered domain while (d) is the area denoted by dotted box in (c). The contours in (c) and (d) delineate the vorticity in the scales larger than 150 km and between 50 and 150 km, with intervals = 1.5×10^{-3} s^{-1}, respectively.

Much like the observational analysis carried out by Houze et al. (2009) on Hurricane Ophelia (2005), there were large numbers of small-scale vorticity anomalies in the center area of the modeled Dolly besides the active VHTs, which could be decayed VHTs or VHTs to be (Figs. 13a and 13b in FZ10; Fig. 1a). For simplicity and generality, such vortices together with VHTs are referred to as convectively induced vorticity anomalies (CVAs) in the current work. Close inspection of the evolution of CVAs in the center area of Dolly indicates that they are indeed three-dimensional entities resulting from bursts of deep moist convection. However, as the convection decays, the three-dimensional entities usually cannot maintain perfect vertical coherency under the effects of the axisymmetric flow and nearby CVAs. Compared to the mid- to upper-level part of the CVAs, the signals of the CVAs are usually robust and maximized at low levels (FZ10). Furthermore, the low-level circulation is an important indicator in the genesis and development of a TC. Therefore, the current study focuses mainly on the evolution of the low-level vorticity associated with CVAs and examines in detail the evolution and multiscale interactions of these CVAs along with their impacts on the genesis and development of Hurricane Dolly. The remainder of this paper is organized as follows. Section 2 presents an overview of the multiscale features in the development of Hurricane Dolly. Sections 3–5 are devoted to discussions of the system-, convective-, and cluster-scale processes that occurred, respectively. Concluding remarks are given in section 6.

2. An overview of multiscale features in the development of Hurricane Dolly

Hurricane Dolly (2008) originated from an African easterly wave. The synoptic analysis based on the National Centers for Environmental Prediction (NCEP) Global Forecast System (GFS) analysis indicates that the precursor of Dolly was always situated in the critical layer of the easterly wave, where the mean flow equals the wave phase speed (FZ10). In the synoptic-scale "pouch" or "sweet spot" for TC formation and intensification (Dunkerton et al. 2008), multiscale processes were active in the developing stage of Dolly, that is, in the period from 1200 UTC 20 July to 1200 UTC 23 July.

Figures 1b–d show the plan view of the relative vorticity at $z = 188$ m[1] (188-m relative vorticity) at different scales at 0300 UTC 22 July when Dolly begins rapid intensification. Separation of the scales is achieved with a two-dimensional spectral decomposition based on fast Fourier transformation (FFT) in Matlab (as in Lin and Zhang 2008).[2] For scales greater than 150 km (hereafter referred to as "system scale"), there is a well-organized but relatively weak vorticity disturbance (Fig. 1b) that is the apparent embryo of Hurricane Dolly. Several well-defined intermediate-scale vorticity anomalies (50 km $< L <$ 150 km) exist and circulate around the primary system-scale vortex (Fig. 1c). Within each of these intermediate-scale positive vorticity anomalies (for example "C1"), there are numerous finer-scale ($L <$ 50 km) vorticity anomalies that are evidently induced by moist convection (Fig. 1d). These small-scale CVAs are of different intensity, some of which may also be

[1] The raw WRF output in the stretched vertical coordinate is interpolated to a linear vertical coordinate started from $z = 188$ m with an interval of 375 m for all diagnostics herein. The first sigma level in the WRF simulation is around 33 m.

[2] In the 2D Fourier decomposition, we divided the total wavenumber ($\sqrt{k^2 + l^2}$) into three scale ranges: i.e., horizontal scales larger than 150 km, between 50 and 150 km, and smaller than 50 km. The frequency response in each given range is 100%, meaning that all signals within the prespecified cutoff frequency (wavenumber) range will be kept while no signals beyond the cutoff frequency will be kept.

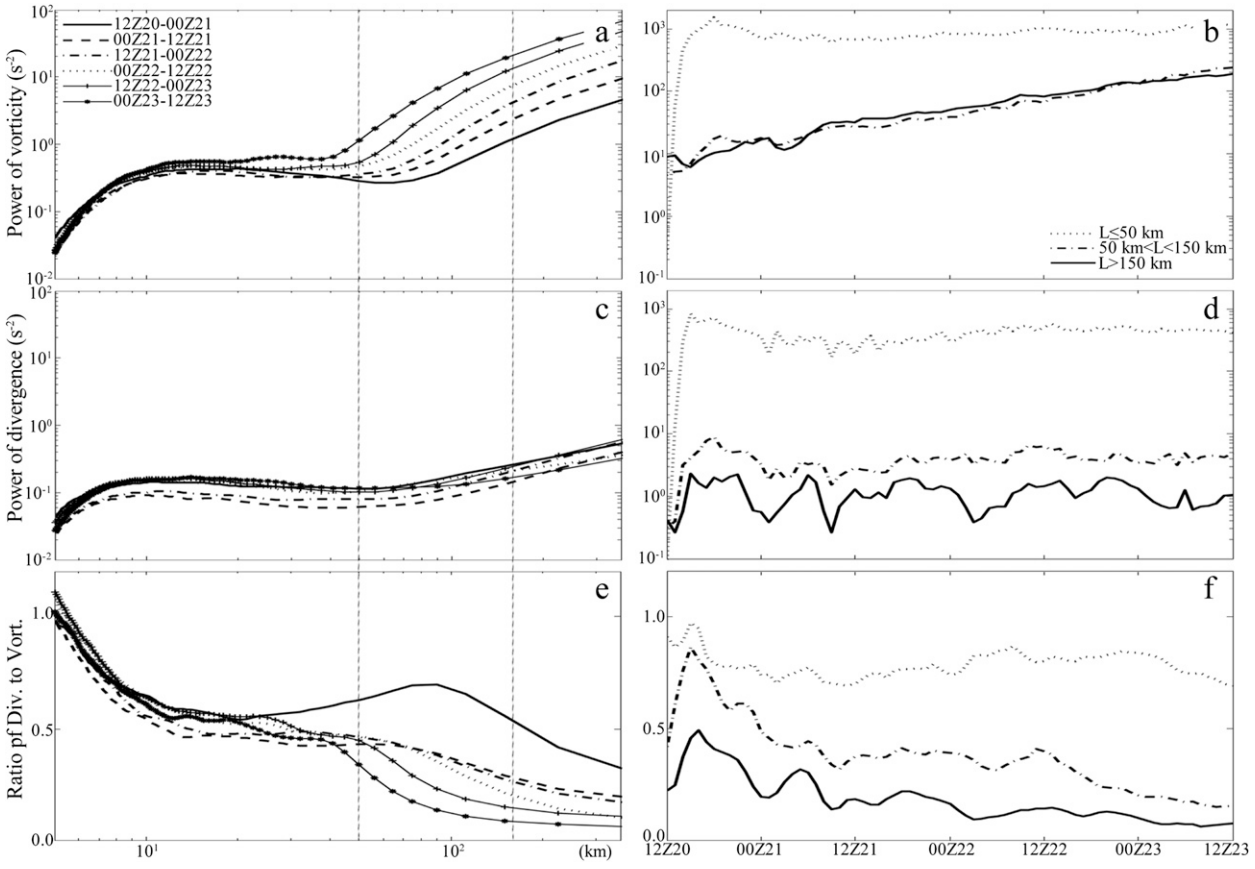

FIG. 2. (a) The 12-h-averaged power spectra of relative vorticity at $z = 1.7$ km. (b) Time evolution of the integrated power spectra of 1.7-km relative vorticity at the three scale ranges. (c),(d) As in (a),(b), but for the divergence at $z = 1.7$ km. (e),(f) As in (a),(b) but for the square root of the ratio of vorticity power to divergence power.

categorized as VHTs, and evolve around their respective intermediate-scale vorticity anomalies. Therefore, each of the intermediate-scale (50 km $< L <$ 150 km) vorticity anomalies may be regarded as a cluster of convective-scale CVAs (hereafter also referred to as ''cluster scale'' vorticity anomalies).

Figure 2a shows the power spectra of relative vorticity at $z = 1.7$ km averaged every 12 h from 1200 UTC 20 July to 1200 UTC 23 July, while Fig. 2b shows the time evolution of the integrated power spectra of vorticity at each of the three distinctive scales (convective scales, $L <$ 50 km; cluster scales, 50 km $< L <$ 150 km; system scales, $L >$ 150 km). The spectral analysis of the corresponding horizontal divergence is shown in Figs. 2c and 2d. The amplitude (spectral power) of the vorticity at nearly all scales below 50 km (i.e., the convective scales) becomes saturated within the first 12 h and remains nearly constant while the amplitudes of the vorticity at the intermediate (cluster scale, ~50–150 km) and system ($L >$ 150 km) scales increase steadily throughout the development of Dolly (Figs. 2a and 2b). Since convection is essential in the transfer of energy from the lower to middle to upper troposphere, saturation of the vorticity at convective scales implies that the continuous production of vorticity through convection, such as VHTs, at these small scales will be transferred immediately upscale to the cluster or system scales.

How does the vorticity grow upscale? Hendricks et al. (2004) proposed that the merger of VHTs typically leads to the upscale transfer of energy while Haynes and McIntyre (1987), and Tory and Montgomery (2008), pointed out that the enhancement of the system-scale vorticity can only be ascribed to the horizontal vorticity flux and vertical momentum transfer occurring in the lateral boundary of the disturbance. These two studies imply that the pure VHT mergers explain only the enhancement of the cluster-scale vorticity but not the strengthening of the system-scale vortex. One possibility for system-scale vortex growth is through the low-level convergence induced by the integrated heating of all convection (under the control of the Sawyer–Eliassen equation) that converges the environmental or convectively generated vorticity toward the

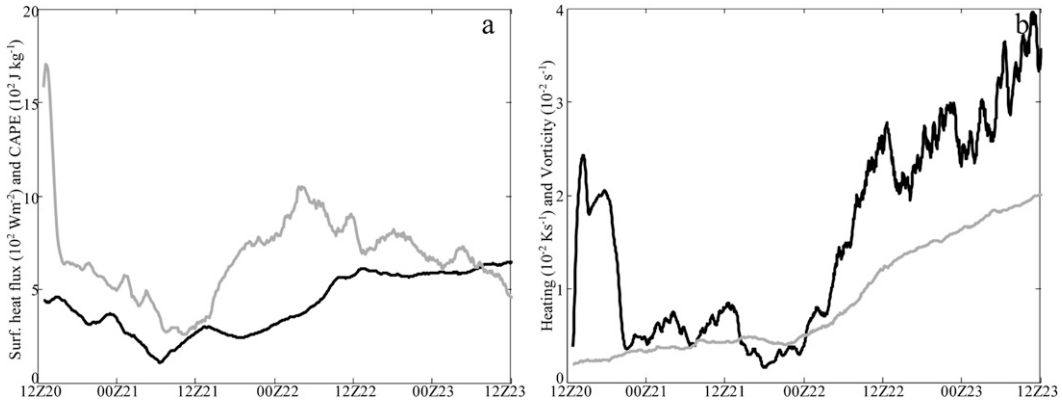

FIG. 3. (a) Time evolution of the total fluxes of sensible and latent heat from the sea surface (black) and the surface-based CAPE (gray) averaged over the storm-centered domain within a radius of 90 km. (b) As in (a), but for the diabatic heating (black) and the vertically integrated relative vorticity (gray).

center of the system-scale vortex. In the following sections, it will be clear that such a process is the primary route to the system-scale development while most merging processes of smaller-scale vortices such as VHTs or CVAs are one of the natural consequences of the system-scale vorticity convergence.

Different from vorticity, the spectral power of horizontal divergence at $z = 1.7$ km reaches near saturation at all scales within the first few hours of model integration started from 1200 UTC 20 July and maintains a similar amplitude throughout the developing stage of Dolly (Figs. 2c and 2d). The persistent increase in vorticity and the nearly steady divergence in the cluster and system scales (Figs. 2a–d) imply that the cluster- and system-scale processes become more rotationally dominant during the development of Dolly (McWilliams 1985; Davis and Emanuel 1991). From Figs. 2e–f, we notice that the square root of the ratio of the divergence power to the vorticity power (scaled as the Rossby number) exhibits an obvious reduction at the cluster and system scales; this ratio is much smaller than 0.5 at the system scale during most of the spinup period of Dolly, suggesting that the simulated development of Dolly becomes increasingly more balanced in the system-scale sense. This is in agreement with the well-held argument in TC dynamics that, to a first order of approximation, the primary circulations of TCs are vortices in near gradient balance (Shapiro and Willoughby 1982; Willoughby 1990).

3. Quasi-balanced evolution of Hurricane Dolly in the system scale

a. Rossby radius of deformation and geostrophic adjustment

The spectral analysis in the previous section suggests that the system-scale vortex is in approximate balance throughout the developing stage of Dolly. How the balance is maintained in such a strong convectively driven system with strong surface heat fluxes, CAPE, and diabatic heating (Fig. 3) is an interesting issue. Chen and Frank (1993) argued that the response of the atmosphere to a local forcing depends on the relative horizontal scales of the forcing and the Rossby radius of deformation. Therefore, the Rossby deformation radius is analyzed as a first step toward understanding the balanced dynamics in the system-scale circulation in the development of Dolly. As far as TCs are concerned, the Rossby deformation radius can be written as (Schubert et al. 1980; Schubert and Hack 1982; Ooyama 1982; Frank 1983)

$$L_R = \frac{NH}{(f+\zeta)^{1/2}(f+2VR^{-1})^{1/2}} = \frac{NH}{I}, \qquad (1)$$

where f is the Coriolis parameter; ζ, V, N, and I, are the mean vertical components of the relative vorticity, tangential velocity, Brunt–Väisälä, and inertial frequencies, respectively; and H and R denote the scale height and horizontal scale of the system. If the scale of a local forcing L is equal to or greater than L_R, a geostrophic adjustment of the wind field to the perturbation of the mass field occurs. While, if L is considerably smaller than L_R, the result is the geostrophic adjustment of the mass field to the wind field.

Figure 4a shows a time–height diagram of the mean I^2 and N^2 averaged in the storm-centered domain within a radius of 90 km. It is evident that the time variation of the mean static frequency N^2 is trivial while the mean inertial frequency experiences significant variations in the developing stage of Dolly. In the first 36 h, the distinct I^2 was mainly confined to the lower troposphere ($<\sim 3$ km) with rather slow growth. After around 0000 UTC 22 July, with the rapid intensification of Dolly, the mean inertial

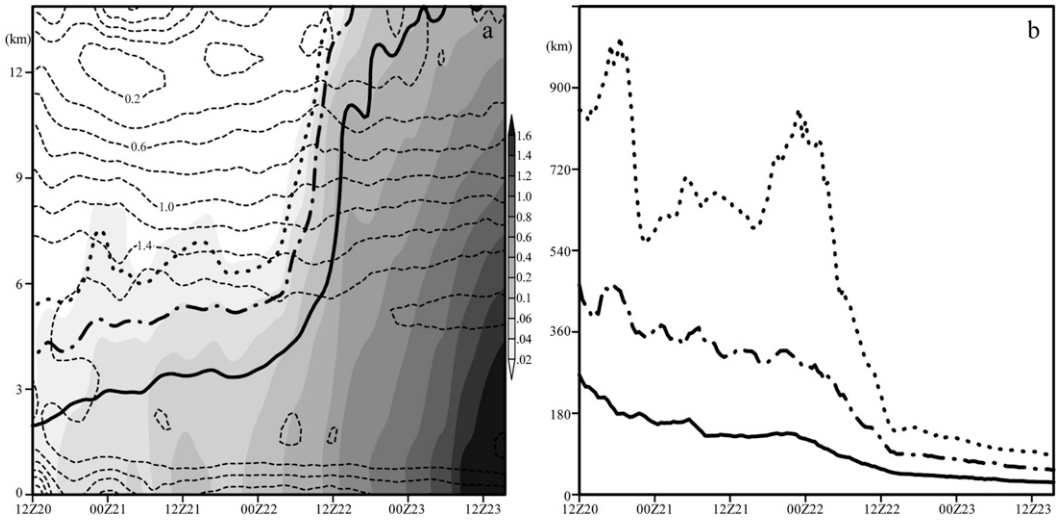

FIG. 4. (a) Time–height diagram for mean I^2 (shaded, interval = 0.2×10^{-6} s^{-2}) and N^2 (dashed contours, interval = 0.2×10^{-4} s^{-2}) averaged over the storm-centered domain within a radius of 90 km. The black solid, dash–dotted, and dotted lines delineate the Rossby deformation radii of 180, 360, and 540 km, respectively. (b) Time variation of the Rossby deformation radii calculated with 0–3-km-mean I and N and a scale height of 3 km (solid line), 0–5-km-mean I and N and a scale height of 5 km (dash–dotted line), and 0–8-km-mean I and N and a scale height of 8 km (dotted line).

frequency increased sharply throughout the whole troposphere. The vertical extension of the mean inertial frequency shown in Fig. 4a indicates that H increases as Dolly spins up, which complicates the calculation of the Rossby deformation radius. For simplicity, the Rossby radii of deformation of values of 180, 360, and 540 km displayed in Fig. 4a are estimated with H, N, and I in Eq. (1) replaced by the altitude and the vertically averaged N and I from the surface to the altitude. We can see that, due to the low-level vorticity maximum, the Rossby radius of deformation is smaller than or comparable to the system scale in the lower troposphere before 0000 UTC 22 July. This indicates that the energy produced by convective heating in the lower to middle troposphere can be efficiently confined to the system-scale vortex instead of propagating away as gravity waves and, correspondingly, the low-level wind field adjusts to balance such thermodynamic perturbations (Raymond and Jiang 1990; Nolan 2007; Nolan et al. 2007; Hawblitzel et al. 2007; Laing and Evans 2010). Therefore, the system-scale vorticity is enhanced gradually at first in the low levels, consistent with the bottom-up development of Dolly proposed in FZ10.

Along with an increase of low-level vorticity on the system scale, the Rossby radius of deformation is reduced gradually and the vortex becomes more efficient in generating rotational momentum by enhancing the conversion efficiency of heating to kinetic energy (Hack and Schubert 1986; Nolan 2007; Nolan et al. 2007). Following 0000 UTC 22 July, the Rossby radius of deformation in most of the troposphere is smaller than the system scale, which indicates that the convective heating released into the troposphere can be effectively trapped within the system-scale vortex and, thus, fuels the storm more efficiently. This results in Dolly's rapid spinup after 0000 UTC 22 July. Figure 4b further shows the time evolution of the mean Rossby radius of deformation with 3-, 5-, and 8-km scale heights, respectively. Coinciding with the development of Dolly, the Rossby radius of deformation in the lower, middle, and upper regions of the troposphere is distinctly reduced and finally became smaller than the system scale, especially after 1200 UTC 22 July. With no substantial variations in system-scale mean static stability, the reduction of the Rossby deformation radius mainly results from the increase of the mean inertial stability. This is consistent with the ''heat trapping'' concept elucidated by Schubert and Hack (1982) and Hack and Schubert (1986), who demonstrated that the conversion of heat energy to kinetic energy becomes more efficient with an increase in the inertial stability of the TC vortex as a whole.

b. Secondary transverse circulation and system-scale development

Based on the spectral analysis and the calculation of the Rossby radius of deformation, the system-scale response that occurred in the development of Dolly could be depicted as a spontaneous adjustment to the area-integrated diabatic heating to remain quasi-balanced. Since the system scale is a well-organized vortex (Fig. 1b), the adjustment processes can be further explored by

diagnosing the axisymmetric secondary circulation forced by diabatic heating through the Sawyer–Eliassen equation (e.g., Schubert et al. 1980; Shapiro and Willoughby 1982; Hack and Schubert 1986; Hendricks et al. 2004; Pendergrass and Willoughby 2009; Willoughby 2009).

Under the constraint of the hydrostatic and gradient wind balance, the Sawyer–Eliassen equation for the toroidal streamfunction ψ in the vorticity-centered[3] domain can be written as (Montgomery et al. 2006)

$$\frac{\partial}{\partial r}\left(\frac{N^2}{r}\frac{\partial \psi}{\partial r} - \frac{\overline{\xi}}{r}\frac{\partial \overline{v}}{\partial r}\frac{\partial \psi}{\partial z}\right) + \frac{\partial}{\partial z}\left(-\frac{\overline{\xi}}{r}\frac{\partial \overline{v}}{\partial z}\frac{\partial \psi}{\partial r} + \frac{\overline{\xi}\,\overline{\eta}}{r}\frac{\partial \psi}{\partial z}\right) = \frac{g}{\theta_0}\frac{\partial \overline{Q}}{\partial r} - \frac{\partial}{\partial z}(\overline{\xi F}), \tag{2}$$

where $\overline{\xi} = f + 2\overline{v}/r$, $\overline{\eta} = f + \overline{\zeta}$, $\overline{u} = -\partial\psi/r\partial z$, $\overline{w} = \partial\psi/r\partial r$, and $\theta_0 = 300$ K. In Eq. (2), the forcing due to heating is defined as $\overline{Q} = -\overline{u'\partial\theta'/\partial r} - \overline{w'\partial\theta'/\partial z} + \dot{\overline{\theta}}$, where the first two terms represent eddy radial and vertical heat fluxes, and $\dot{\overline{\theta}}$ is the azimuthal-mean diabatic heating rate. The momentum forcing is defined similarly as $\overline{F} = -\overline{u'\zeta'} - \overline{w'\partial v'/\partial z} + \overline{F}_{sg}$, where the first two terms represent the eddy radial vorticity and eddy vertical momentum fluxes, respectively, and $\overline{F}_{sg}$ is the term owing to the diffusive and surface-layer processes in the numerical model. Equation (2) implies that, under the constraint of thermal wind balance, the heating and momentum forcing will induce the secondary circulation, which plays a vital role in the intensification of TCs.

As in Montgomery et al. (2006), both $\dot{\overline{\theta}}$ and $\overline{F}_{sg}$ are calculated as the residual terms in the azimuthal mean thermodynamic and tangential momentum equations, respectively, and the zero normal flow along the $r - z$ boundary of the vortex is taken as the boundary condition; that is, $\psi = 0$ along the $r - z$ boundary. If the solvability criterion

$$N^2\,\overline{\xi}\,\overline{\eta} - \left(\overline{\xi}\frac{\partial \overline{v}}{\partial v}\right)^2 > 0 \tag{3}$$

remains satisfied throughout the fluid, Eq. (2) is elliptic and a unique solution for ψ is guaranteed (Shapiro and Willoughby 1982) and can be achieved through standard successive overrelaxation (SOR; Press et al. 1992). In regard to the developing phase of Dolly, the solvability criterion [Eq. (3)] is violated only locally in the upper troposphere, at which point a regularization procedure on the azimuthal-mean tangential velocity is performed to obtain a convergent solution.

Figures 5a–d shows the WRF-simulated azimuthal-mean radial and vertical velocity averaged over the period of ~0000–1100 UTC 21 July, ~1200–2300 UTC 21 July, ~0000–1100 UTC 22 July, and ~1200–2300 UTC 22 July, respectively. Evidently, this illustrates the gradual strengthening of the azimuthal-mean low-level inflow and updraft and upper-level outflow, along with the spinup of Dolly. Though the upper-level outflow is comparatively weaker than that simulated by the WRF, the basic structure and evolution of the axisymmetric components (i.e., the radial inflow and updraft) are successfully captured by the Sawyer–Eliassen model (Figs. 5e–h). This is consistent with findings from the spectral analysis that the system-scale vortex of Dolly maintains approximate gradient balance. From Figs. 5e–h, one notices that, under the heating and momentum forcing in combination with the constraint of the inherent thermal wind balance, considerable system-scale convergent inflow developed in the lower troposphere. This is also consistent with the foregoing analysis on the Rossby radius of deformation; that is, under the condition that the Rossby radius of deformation is smaller than the system scale, considerable adjustment of the wind field will occur to balance the changes in the thermodynamic field induced by the thermal forcing. The vertical vorticity budget averaged over the inner core of Dolly, performed in FZ10, suggests that the enhancement of the low-level vorticity is mainly ascribed to the stretching effect, which converges the ambient vorticity into the inner-core area within the boundary layer. From Figs. 5a–h, it can be inferred that the convergent flow associated with stretching results from the near-spontaneous balance response of the system-scale vortex to the heating and momentum forcing.

Figures 5i–l shows the azimuthal-mean radial and vertical velocities induced by the eddy fluxes and subgrid processes, also through the Sawyer–Eliassen equation. Comparing Figs. 5i–l with Figs. 5a–d and 5e–h, it is evident that, although the eddy fluxes and subgrid processes do contribute to the development of the secondary circulation in the development of Dolly, the resulting updraft, and low- and upper-level radial flows, are much weaker than those obtained in the WRF simulation. Therefore, the spinup of the system-scale secondary circulation mainly results from the axisymmetric diabatic heating, as suggested by Nolan and Grasso (2003), Nolan et al. (2007), and Montgomery et al. (2006).

The resemblance between Figs. 5a–d,e–h stands in contrast to Bui et al. (2009), who argued that the friction

[3] To minimize the impacts of the small-scale deep moist convection on the location of the vorticity center, a filter based on the two-dimensional spectral decomposition (Lin and Zhang 2008) is performed on the vorticity field at the lowest model level (z = 188 m) to filter the perturbations with horizontal scale less than 270 km. The location with the maximum vorticity in the filtered field is taken as the vorticity center. Also see footnote 2.

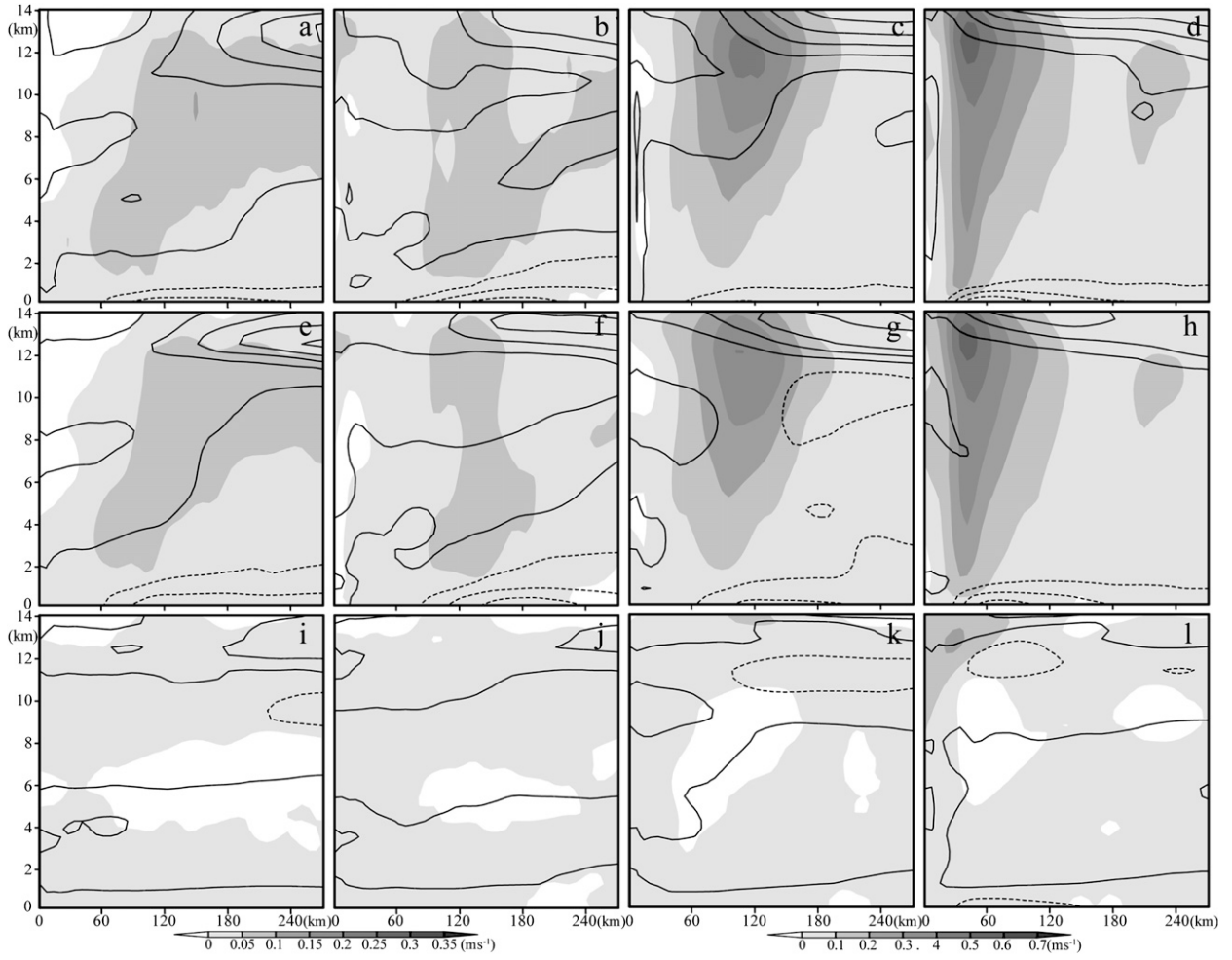

FIG. 5. (a)–(d) Radius–height diagram for the WRF-simulated azimuthal-mean radial velocity (contours, interval = 1 m s^{-1}) and vertical velocity (shading) averaged during the period (a) ~0000–1100 UTC 21 Jul, (b) ~1200–2300 UTC 21 Jul, (c) ~0000–1100 UTC 22 Jul, and (d) ~1200–2300 UTC 22 Jul 2008. (e)–(h) As in (a)–(d), but for the radial and vertical velocities derived from the Sawyer–Eliassen equation. (i)–(l) As in (e)–(h), but the Sawyer–Eliassen equation is forced only by the eddy fluxes and subgrid processes. Negative contours are dashed.

in the boundary layer might lead to considerable deviation of the Sawyer–Eliassen equation solution from the model-derived secondary circulation. This could be ascribed to the fact that Dolly is a rather weak hurricane. The PV inversion performed by Zhang and Kieu (2005) also indicated that, in the eyewall region, the vertical motion induced by the boundary layer processes is significantly weaker than that from diabatic heating.

To further illustrate the role of the thermal forcing in the spinup of Dolly, two idealized simulations based on the axisymmetric hurricane model developed by Rotunno and Emanuel (1987) are performed. In these idealized experiments, the initial vortex is in thermal wind balance, with the tangential velocity being equal to the azimuthal-mean tangential velocity derived from the WRF at 1200 UTC 20 July. The axisymmetric hurricane model is forced directly by the heat forcing estimated from the WRF simulation. Two forms of the thermal forcing are adopted; that is, $\overline{Q} = -\overline{u'\partial\theta'/\partial r} - \overline{w'\partial\theta'/\partial z} + \dot{\bar{\theta}}$ and $\overline{Q}_1 = \dot{\bar{\theta}}$. The former is exactly the same as that in Eq. (2) while the eddy heat flux is omitted in the latter. Since the heat forcing derived from the WRF output has included the contribution from the sea surface, the sensible heat and moisture fluxes from the ocean are turned off in the idealized experiments. Figure 6 displays the time–radius diagrams for the axisymmetric tangential velocity at 1.5 km simulated by WRF and the idealized hurricane model. It is evident that the axisymmetric tangential velocity simulated by the idealized model exhibits a strengthening tendency comparable to that derived from the WRF. The reproduction of the tangential velocity by the idealized model with only azimuthal-mean diabatic heating (Fig. 6c)

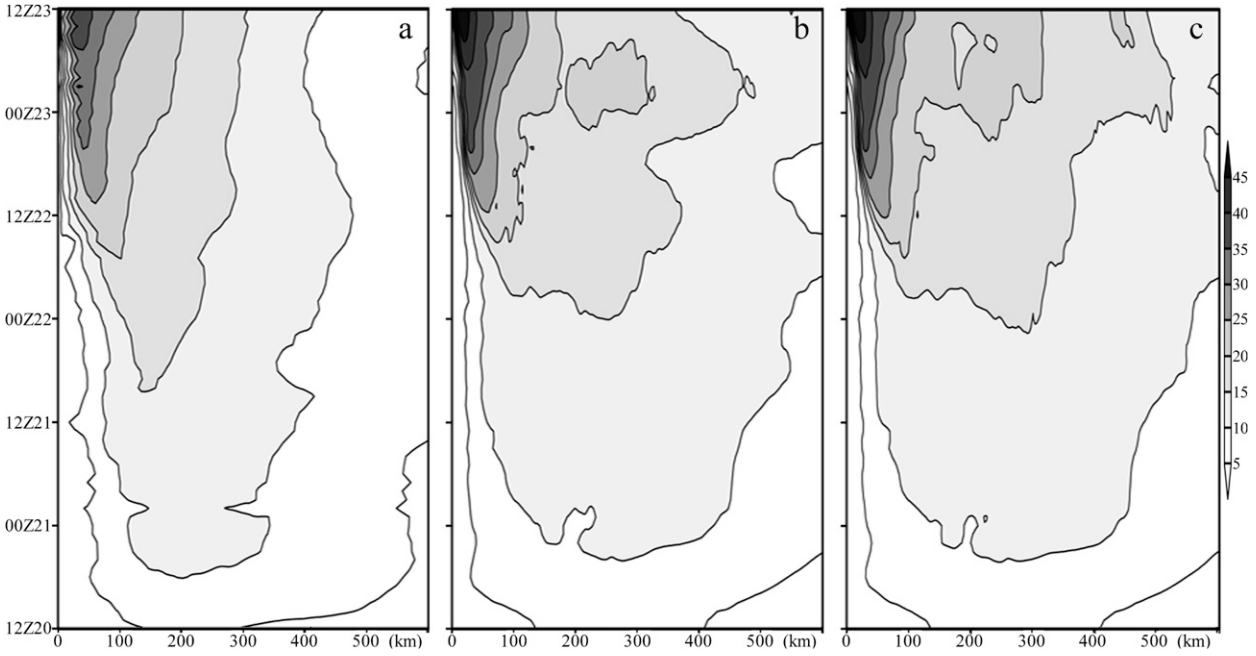

FIG. 6. (a) Time evolution of WRF-simulated azimuthal-mean tangential velocity (m s^{-1}) at $z = 1.5$ km. (b) As in (a), but for the tangential velocity obtained by integrating the Rotunno and Emanuel (1987) model that is driven by the heating derived from WRF. (c) As in (b), but the symmetric heating resulting from the eddy fluxes is omitted.

further demonstrates that the system-scale diabatic heating plays a vital role in the development of Dolly. The slightly stronger tangential velocity simulated by the idealized model is likely due to the omission of the asymmetric processes (Wu and Braun 2004) or due to the physics/numerical differences between the two models. Results from the 2D idealized experiments are also consistent with Nolan and Grasso (2003) and Nolan et al. (2007), showing that the symmetric response to the purely asymmetric part of the heating has a very small and most often negative impact on the intensity of the vortex.

c. *Relation between smaller-scale convection and system-scale CAPE and diabatic heating*

Although the diagnosis based on the Sawyer–Eliassen equation and the idealized experiments with the 2D axisymmetric model indicates that asymmetric forcing, which is usually associated with smaller-scale processes, might be peripheral to the development of the secondary circulation and subsequent intensification of the system-scale vortex, the importance of smaller-scale processes such as small-scale cumulonimbus towers in the development of Dolly should not be underestimated. This subsection explores the relationship between smaller-scale (convective) processes and the system-scale CAPE and diabatic heating.

Figure 7 summarizes the statistics of the vertical velocity and diabatic heating in the storm-centered domain of Dolly within a radius of 90 km. It shows distributions of the 12-h mean frequency of occurrence for values of vertical velocity and diabatic heating as a function of height, that is, the contoured frequency by altitude diagram (CFAD).[4] With reference to Figs. 3 and 7, it can be seen that the spinup process of Dolly in the system scale is quite similar to that described by Rotunno and Emanuel (1987). In the first 12-h simulation, as the vortex winds pass over the warm ocean surface, heat and moisture are transferred into the atmosphere and produce locally higher conditional instability and, subsequently, convection and latent heat release (Figs. 3a, 7a, and 7e). Simultaneously, the system-scale vorticity increased gradually as a result of the spontaneous adjustment (Fig. 3b). However, as the cool and dry midlevel air descends to the surface from the mid- to upper-level dry-air intrusion (FZ10), convective activity slows and the release of CAPE and diabatic

[4] CFAD was first used by Yuter and Houze (1995) to analyze the evolution of vertical motion and reflectivity in a midlatitude mesoscale convective system (MCS) and has recently been introduced into the study of TCs (e.g., Black et al. 1996; Rogers et al. 2007; Nolan 2007; Zhang and Sippel 2009; FZ10). In this study, CFAD was produced in a similar manner to that in Nolan (2007). The values of vorticity at each altitude in a 90-km-radius circle around the center of the incipient Dolly were divided into 20 equal bins between the values shown on the x axis in the plot. To better view the large range of frequency values in these two-dimensional contour plots, we add 1 to the frequency values everywhere and then take the base 10 logarithm of the sum.

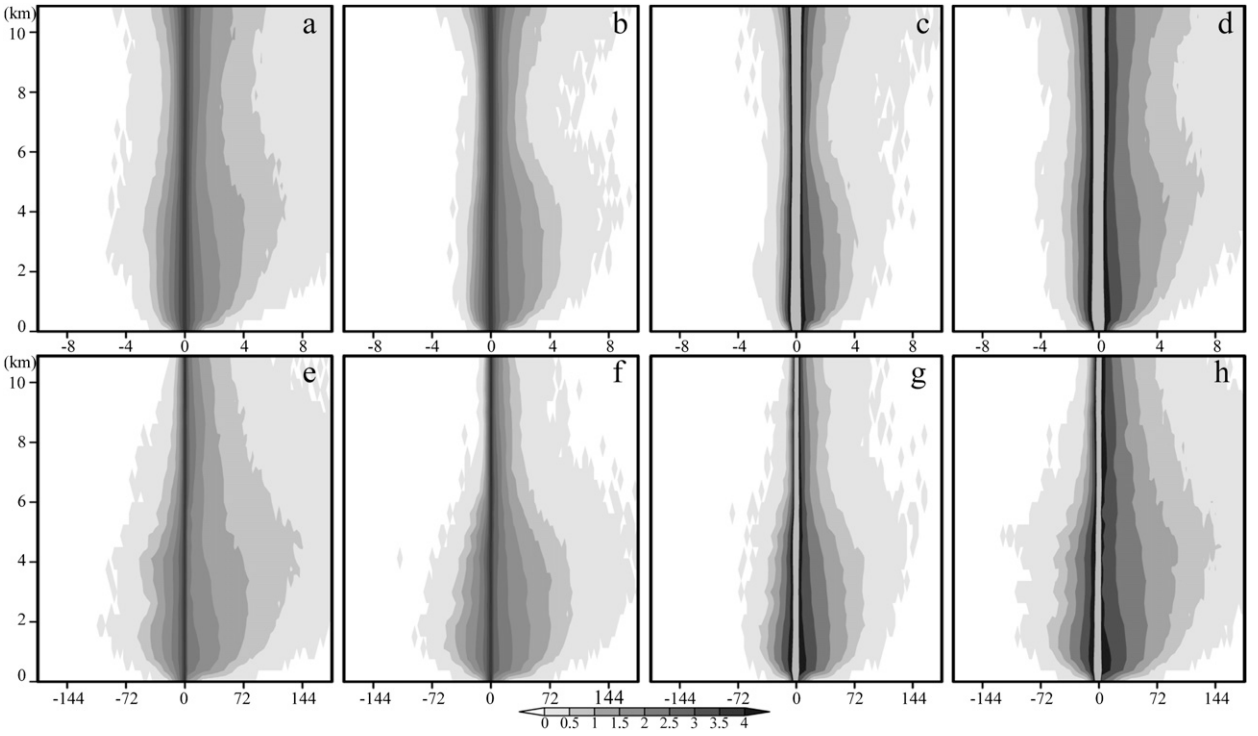

FIG. 7. (a)–(d) Contoured mean frequency altitude diagrams for the vertical velocity (x axis, m s^{-1}). The mean frequency is obtained by averaging the frequency in the period of (a) ~1200–2300 UTC 20 July, (b) ~0000–1100 UTC 21 July, (c) ~1200–2300 UTC 21 July, and (d) ~0000–1100 UTC 22 July. (e)–(h) As in (a)–(d), but for the diabatic heating (x axis; K h^{-1}).

heating becomes weak (Figs. 3a, 7b and 7c, and 7f and 7g). In the period from ~1200 UTC 21 July to ~0400 UTC 22 July, the surface-based CAPE accumulates as a result of the surface heat and moisture fluxes (Fig. 3a). Renewed vigorous convection then produced condensational heating, which enhanced the system-scale vortex throughout the troposphere (Figs. 3, 7d, and 7h). As a result, a steadily amplifying circulation developed after about 0400 UTC 22 July.

The above analysis suggests that smaller-scale processes, including individual convective towers, are vital elements of the developing system and may contribute significantly to the collection, conversion, release, and transfer of heat (thermal energy) to the system scale. The following section will analyze these smaller-scale convective processes in detail to further understand the intensification of Dolly.

4. Convective-scale processes occurred in the development of Hurricane Dolly

Smaller-scale convective processes, especially VHTs, have been the subject of many recent studies on the development of TCs (e.g., Hendricks et al. 2004; Montgomery et al. 2006, 2009; Nguyen et al. 2008). There were also numerous active VHTs in the development of Dolly, each of which had a lifespan on the order of 1 h. However, there exist many other modes of moist convection, including boundary layer rolls, shallow convection, and decaying or remnant VHTs, all of which may contribute to the wide range of vorticity anomalies (e.g., Figs. 13a and 13b in FZ10 and Fig. 1a). As mentioned earlier, we label all these small-scale features more generally as CVAs, as a generalization of VHTs.

To help understand the evolution and influence of convective-scale CVAs on the development of Dolly, three such CVAs are tracked. Figure 8 shows the tracks of three CVAs that first appear at 0304, 2314, and 2334 UTC 21 July, which are referred to, respectively, as CVA-0304, CVA-2314, and CVA-2334 in the TC-following reference framework. CVA-0304 initially spirals radially inward, then outward, and later inward again, before eventually wrapping itself around the storm center at a radius of less than 50 km. Both CVA-2314 and CVA-2334 first appear northeast of the storm center and spiral directly toward the center, each of which eventually circles around the center at a radius similar to that of CVA-0304. Unlike a typical VHT that has a lifespan on the order of 1 h, these CVAs can be long lived through repeated cycles of convective development as well as decay or through

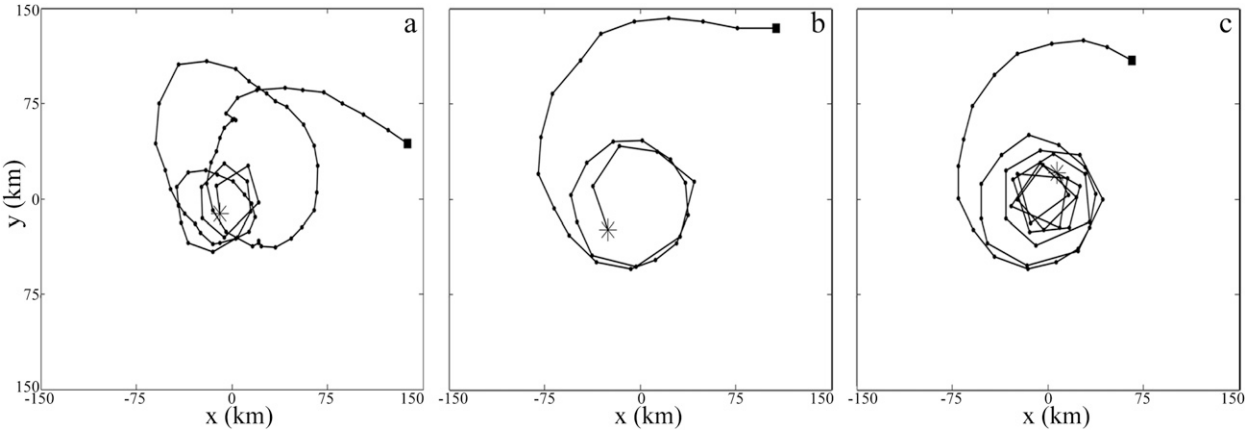

FIG. 8. Tracks of CVAs originated at approximately (a) 0304, (b) 2314, and (c) 2334 UTC 21 July. The tracks are ended at 1604, 2214, and 2323 UTC 22 July, respectively. The squares and stars denote the beginning and the ending of each track. Interval along trajectories denoted by black dots is 30 min.

mergers. Figure 9 summarizes a variety of processes that occurred during the life cycle of CVA-0304 and the corresponding evolution of vorticity, respectively.

a. Merger of VHTs and its relation to the moist convection

As in Hendricks et al. (2004) and Montgomery et al. (2006), there are apparent mergers of CVAs in the development of Dolly. From 0704 to 0744 UTC 21 July, a distinct merger event associated with CVA-0304 occurs. At 0704 UTC 21 July, an evident CVA (denoted as A2 in Fig. 9a) appears southwest of the original CVA-0304 (A1 in Fig. 9e). About 15 min later, a new CVA emerges between CVA-0304 and A2 (Fig. 10b), through which CVA-0304 eventually reaches A2. For simplicity, the merged anomaly is still labeled as CVA-0304. After the merger, the vorticity of CVA-0304 is remarkably enhanced.

To better understand the increase of vorticity associated with the merger, the relative vorticity budget is performed

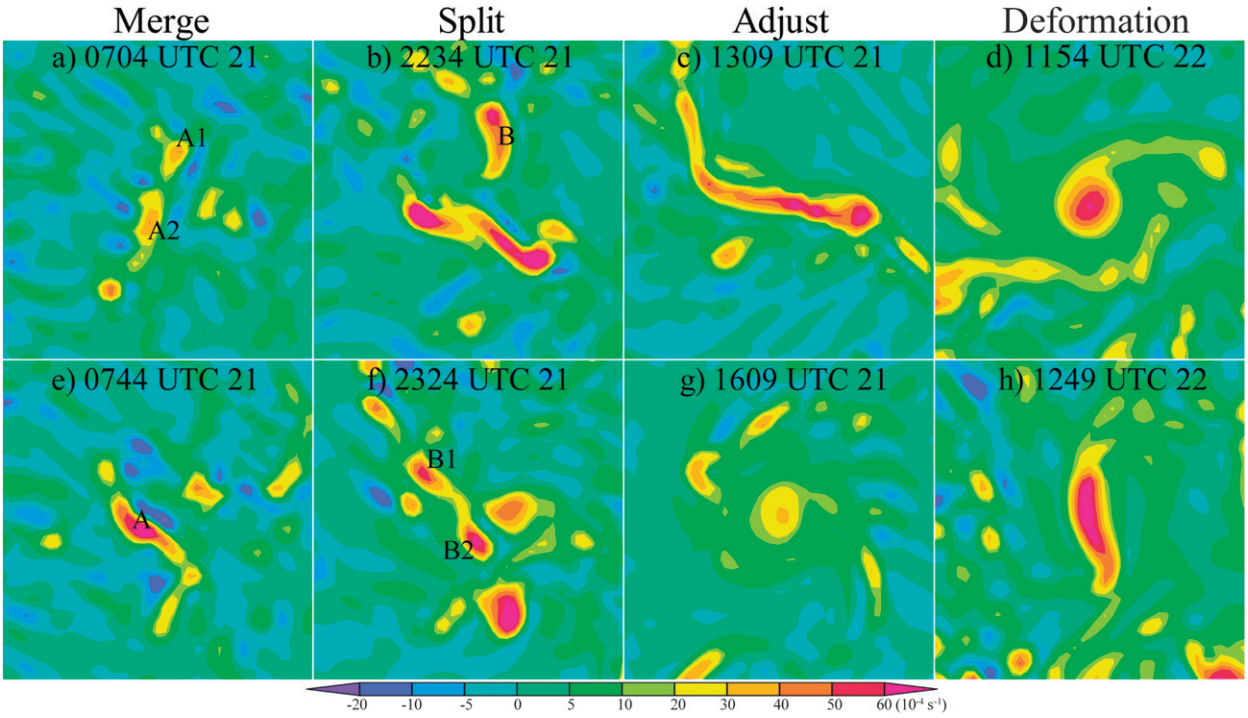

FIG. 9. Main processes occurred in the life cycle of the CVA that originated at ~0304 UTC 21 July (CVA-0304). Shading denotes the 188-m relative vorticity and the domain size is 60 km × 60 km.

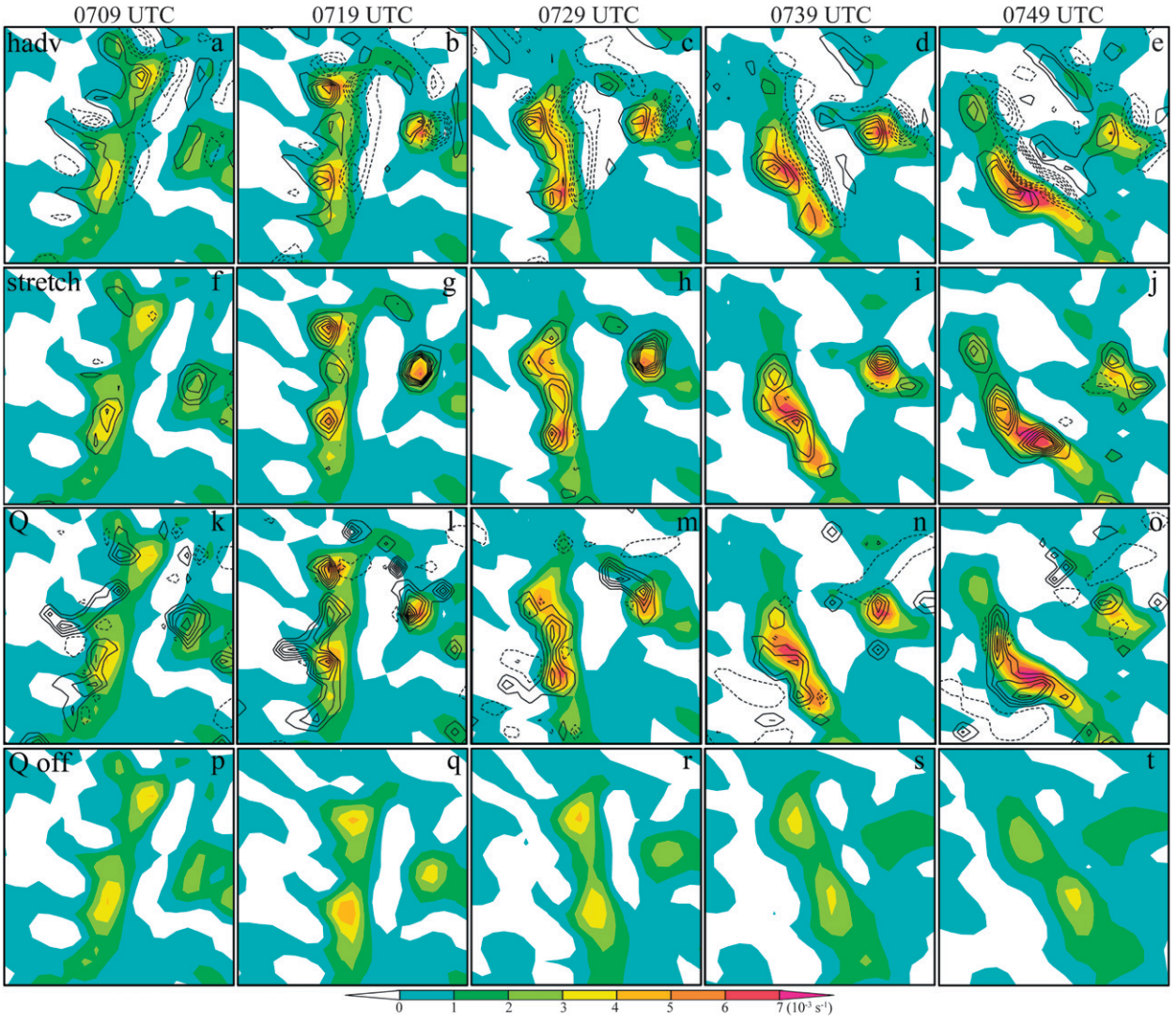

FIG. 10. (a)–(e) Evolution of the vorticity anomalies A1 and A2 in Fig. 9a from 0709 UTC 21 July every 10 min. Shading denotes the relative vorticity (interval = 10^{-3} s^{-1}) and contours denote the vorticity tendency induced by the horizontal advection at z = 188 m (interval = 5×10^{-6} s^{-2}). (f)–(j) As in (a)–(e), but for the vorticity (shaded) and vorticity tendency induced by the stretching effect (contours, interval = 2×10^{-6} s^{-2}). (k)–(o) As in (a)–(e), but for the vorticity (shaded) and diabatic heating (contours, interval = 10^{-3} K s^{-1}). (p)–(t) As in (a)–(e), but for the vorticity (shaded) obtained in the sensitivity experiment without the microphysics processes after 0704 UTC 21 July. The contours of the value of zero are omitted and negative values are dashed.

for CVA-0304 and its nearby area between 0709 and 0749 UTC 21 July. The vorticity equation in a reference frame moving with Dolly (with subscript SR) is adopted and can be written as

$$\left.\frac{\partial \zeta}{\partial t}\right|_{\mathrm{SR}} = -(\mathbf{V}_h - \mathbf{C}) \cdot \nabla_h(\zeta + f) - w\frac{\partial \zeta}{\partial z} - (\zeta + f)\nabla_h \cdot (\mathbf{V}_h - \mathbf{C}) - \left(\frac{\partial w}{\partial x}\frac{\partial v}{\partial z} - \frac{\partial w}{\partial y}\frac{\partial u}{\partial z}\right) + \frac{\partial F_y}{\partial x} - \frac{\partial F_x}{\partial y}, \quad (4)$$

where ζ is the relative vertical vorticity and $\mathbf{C}$ is the moving speed of Dolly determined by the displacement of the large-scale vorticity center. The mean values are approximately -7.4 and 3.1 m s^{-1} in the zonal and meridional directions, respectively (FZ10). The terms on the right-hand side of Eq. (4) represent the contributions to the change of ζ due to horizontal advection of absolute vorticity, vertical advection, stretching, tilting, and subgrid-scale flux derivatives, respectively. The solenoidal terms generally yield minimal contributions to the

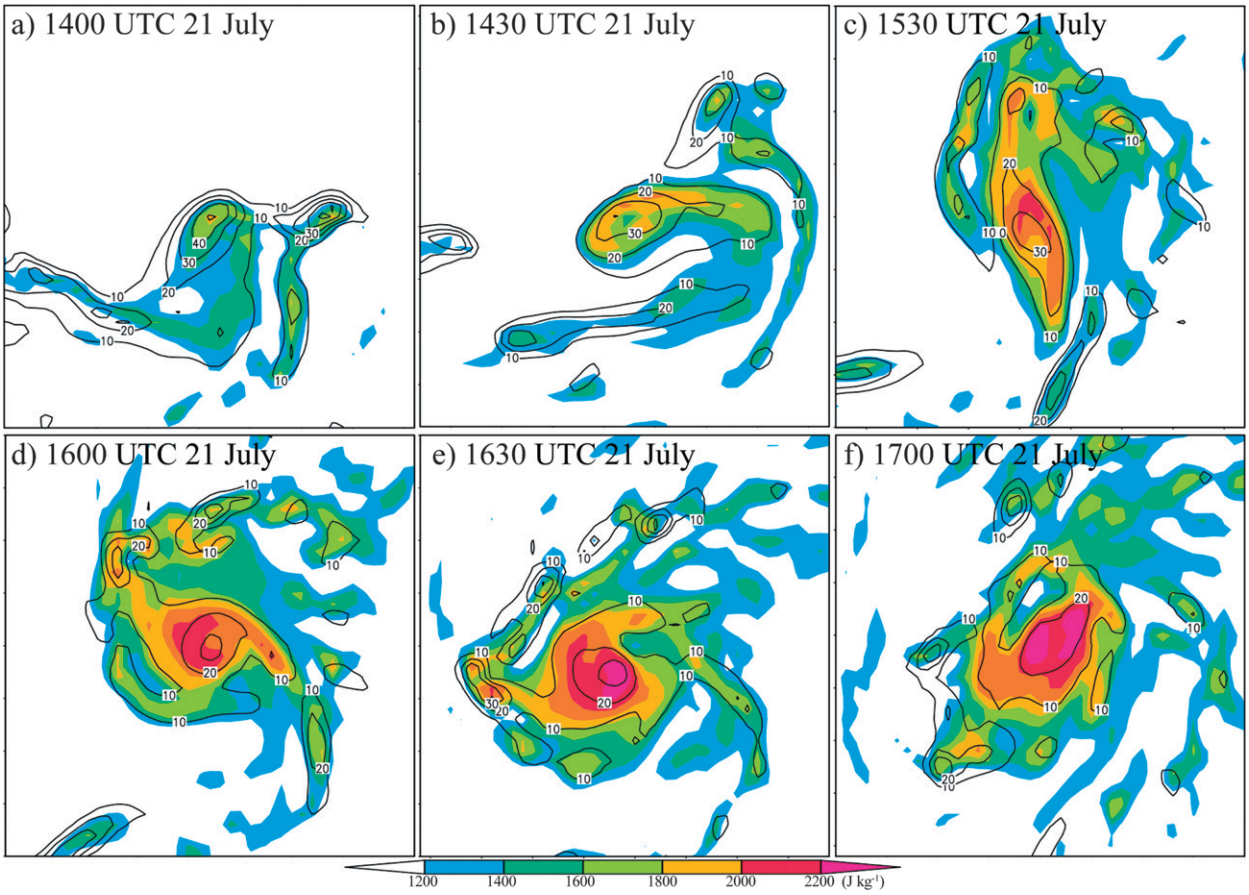

FIG. 11. Evolution of the 188-m relative vorticity (contours) and surface-based CAPE (shading) associated with CVA-0304 at (a) 1400, (b) 1430, (c) 1530, (d) 1600, (e) 1630, and (f) 1700 UTC 21 July. The domain size is 60 km × 60 km.

net vorticity tendency, which have been ignored in Eq. (4) following Montgomery et al. (2006). For simplicity, only the vorticity at $z = 188$ m is considered in the vorticity budget. Therefore, the vertical advection and tilting terms in Eq. (4) are relatively small due to the weak vertical velocity near the surface.

Figures 10a–e display the vorticity tendency induced by the horizontal advection from 0709 to 0749 UTC 21 July every 10 min. It can be shown that the distinct positive and negative vorticity tendencies induced by the horizontal advection were exactly situated on the downwind and upwind sides of the maximum cyclonic vorticity center, respectively. This implies that the effects of horizontal advection on CVA-0304 and the vorticity anomalies nearby act to advect them downwind. Due to the relatively strong horizontal advection of vorticity south of CVA-0304, this CVA approaches A2 gradually. By 0749 UTC 21 July, it seems that the merger of CVA-0304 and A2 has occurred, resulting in a larger and stronger CVA. Since the pure merger of CVAs via horizontal advection and diffusion cannot lead to the increase of vorticity, there must be other processes participating in the merger that are responsible for the distinct enhancement of the CVA.

Differing from the vorticity tendency arising from horizontal advection, the positive vorticity tendency induced by the stretching effect always coincides with an area of large vorticity values (Figs. 10f–j) and is nearly coincident with considerable diabatic heating (Figs. 10k–o). The superposition of the diabatic heating and stretching effects with the evident vorticity implies that the moist convection makes a vital contribution to the enhancement of the CVA's vorticity during the merging process through stretching. This result can be further verified with the aid of Figs. 10p–t, which give the evolution of the vorticity as that in Figs. 10a–e with the exception that the moist processes are turned off after 0704 UTC 21 July. It is obvious that, as far as CVA-0304 is concerned, only the horizontal advection and diffusion in the merger of CVAs are inefficient in the vortex growth: before the merger occurs, the CVAs have weakened considerably. This is consistent with recent findings of

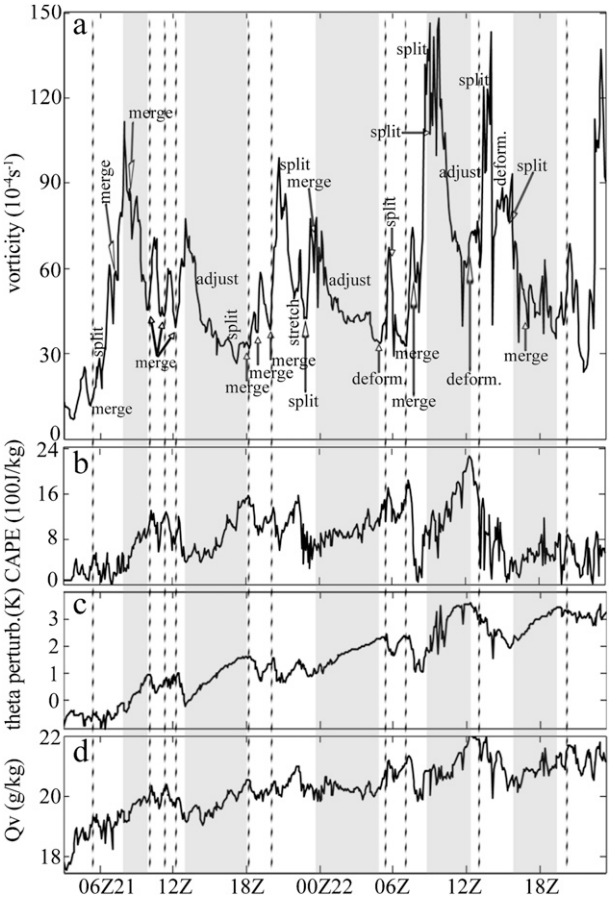

FIG. 12. Time evolution of (a) maximum relative vorticity of the CVA-0304 at $z = 188$ m, (b) the mixed-layer CAPE, (c) potential temperature perturbation at $z = 188$ m, and (d) mixing ratio at $z = 188$ m.

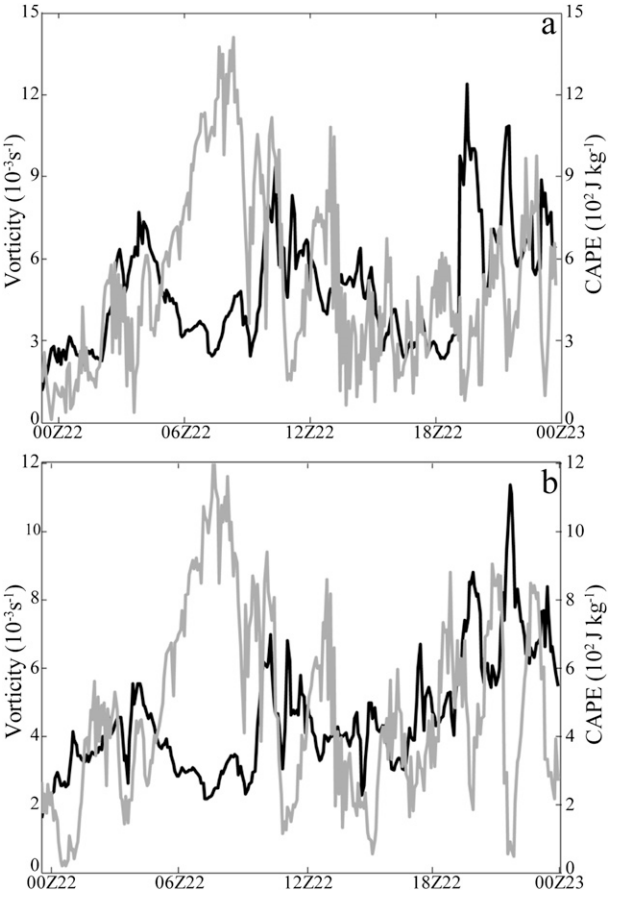

FIG. 13. Time evolution of the maximum relative vorticity at $z = 188$ m (black) and mixed-layer CAPE (gray) for (a) CVA-2314 and (b) CVA-2334.

Nolan (2007). Comparing Figs. 10k–o,p–t, it can be found that the merger of the original CVA-0304 with A2 is mainly ascribed to the moist convection burst between them, which facilitates the merger through the concomitant low-level convergent flow (Hendricks et al. 2006) and enhancement of the vorticity between the CVAs.

Although both the size and intensity of CVA-0304 usually increase in response to the merger processes, CVA-0304 does not continuously intensify via mergers with surrounding CVAs. In fact, due to the deformation and shear associated with the system-scale field and the interactions between CVAs, the split of CVAs also frequently happens in the development of Dolly. As an example, Figs. 9b and 9f shows an episode of splitting that happened during the lifetime of CVA-0304. From 2234 UTC 21 July, the vorticity at the southern tail of CVA-0304 enhances as a result of the new burst of convection. Under the impacts of the environmental wind and the CVAs nearby, CVA-0304 splits into two vorticity anomalies (B1 and B2 in Fig. 9f). The title ''CVA-0304'' is then carried on by the CVA denoted with ''B2'' in Fig. 9f.

b. Adjustment and deformation of the CVAs

After the rapid intensification following the burst of convection or the merger events, CVAs usually experience an adjustment process such as shown in Figs. 9c and 9g. At 1309 UTC 21 July, CVA-0304 develops into a long and strong vorticity anomaly, resulting from a series of merger events and the deforming effects of the environmental wind. In the following 3 h, CVA-0304 evolves through self-adjustment and finally develops into a well-defined circular vorticity anomaly at a larger scale. During this process, the vorticity of CVA-0304 is significantly weakened while the surface-based CAPE around the center of CVA-0304 is remarkably increased (Fig. 11). The maximum value of CAPE increases from around 1600 J kg^{-1} at 1400 UTC July to 2200 J kg^{-1} at 1630 UTC 21 July. It is argued that the cyclonic circulation associated with CVA-0304 spreads horizontally along with the adjustment process (Fig. 9g) and, subsequently, leads

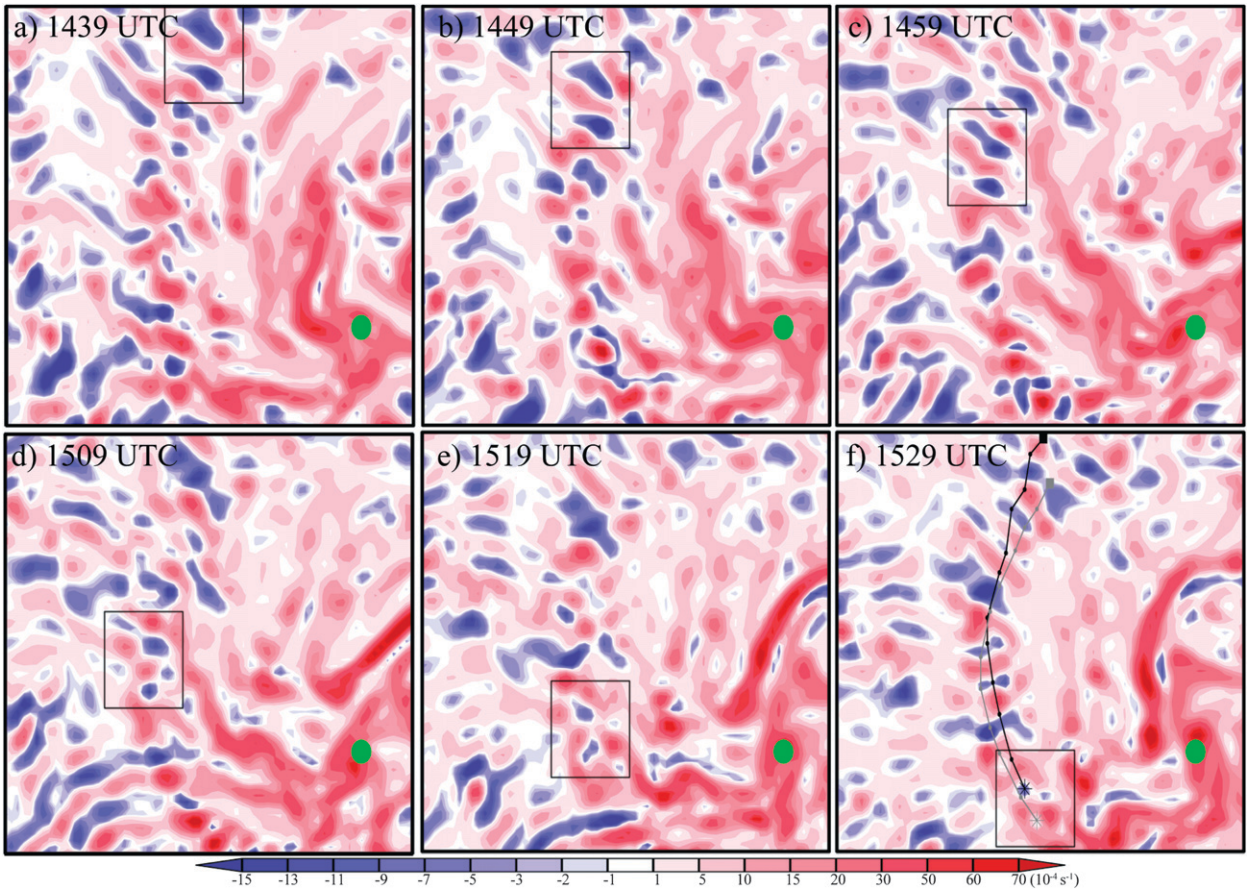

FIG. 14. Time evolution of the 188-m relative vorticity (shading) in the northwestern quadrant of Dolly during ~1439–1529 UTC 22 July. The green dot and the small box denote the storm center and the position of the related negative vorticity anomalies, respectively. The black and gray lines in (f) denote the trajectories of the negative vorticity anomalies in the box. The plotting domain size is 82.5 km × 82.5 km.

to a considerable increase in CAPE in the ambient environment of CVA-0304 via the air–sea interaction (Emanuel 1986). The distinct enhancement of CAPE provides favorable conditions for the development of new convection around this CVA.

As a result of the burst of new convection fueled by the accumulated CAPE, the well-defined small-scale circular vortex as displayed in Fig. 9g could break up into several new CVAs. Provided that the ambient flow is strong enough, it also could be stretched and deform again. At 1154 UTC 22 July, CVA-0304 was a very circular vortex (Fig. 9d) while, about an hour later, it deforms into a long, winding, and narrow vorticity anomaly (Fig. 9h). The intensification of the CVA accompanying the deformation is explained by the release of CAPE that occurred in this process and the concomitant stretching effects.

As a summary, Fig. 12 displays the time evolution of the maximum vorticity, mixed-layer CAPE, lowest-level potential temperature perturbation, and mixing ratio associated with CVA-0304. Contrary to the arguments that the merger event makes a prominent contribution to the increase of a CVA's vorticity, the maximum vorticity of CVA-0304 demonstrates considerable undulation instead of the persistent enhancement, despite frequent mergers that occurred during the lifetime of CVA-0304 (Fig. 12a). Comparing Fig. 12a with Fig. 12b, it can be seen that the sharp strengthening of the CVA is usually accompanied by a sudden decrease in CAPE (dashed lines in Fig. 12b) and followed by a considerable reduction in the maximum vorticity of the CVA (shaded area in Fig. 12a) associated with the adjustment process illustrated in Figs. 9c and 9g. During the adjustment, the low-level potential temperature, mixing ratio, and CAPE increase gradually as a result of the air–sea interaction and surface fluxes (Figs. 12c and 12d). Such a negative correlation of the maximum vorticity and CAPE can also be identified in the evolution of CVA-2314 and CVA-2334 (Fig. 13). The adjustment process mentioned above is also evident for the system-scale vortex in Fig. 3, which shows that the volume-integrated vorticity on the system-scale increases

gradually, coinciding with the release of CAPE in the first 24 h, and then experiences a brief episode of reduction accompanying the sharp increase of CAPE. After around 0400 UTC 22 July, the release of system-scale CAPE occurs again and the system-scale vorticity demonstrates a significant enhancement accordingly.

The above examples of CVA-0304, CVA-2314, and CVA-2334 indicate that many complicated processes may take place during the lifetime of robust CVAs. Along with these processes, CVAs strengthen and decay alternatively, in coincidence with the release and accumulation of CAPE. This suggests that the convective-scale CVAs play a distinct role in the collection and accumulation of CAPE, which is favorable in furthering the burst of new convection. This is similar to the system-scale vortex to a certain extent. In addition, the fact that the individual convective cells can lead to the transient enhancement of CVAs and facilitate the merger of CVAs via the self-induced convergent flow is similar to what occurred on the system scale. In the macroscope, the heating resulting from convection induces instantaneous adjustment of the wind field to the mass field in the system scale through the secondary circulation, the horizontal branch of which converges the environmental vorticity and CVAs into the storm-centered area and causes the system-scale vortex of Dolly to develop gradually.

c. *Evolution of negative vorticity anomalies*

With the development of cyclonic CVAs induced by convection, remarkable negative CVAs are also produced through the tilting and stretching effects, as is also the case in Davis and Bosart (2006). The evolution of such negative vorticity anomalies in the development process of a TC is another interesting issue associated with the CVAs. This section examines the evolution of negative vorticity anomalies that also result from moist convection along with cyclonic CVAs during the development of Dolly.

Figure 14 shows the plan view of the 188-m relative vorticity in the northwestern quadrant of Dolly from 1439 to 1529 UTC 22 July. At 1439 UTC, two noticeable negative CVAs are situated near the northern boundary of the domain of interest. Instead of moving away from the storm center (green dot in Fig. 14), both negative CVAs spiral toward the storm center together with the cyclonic CVAs nearby (Fig. 14f). Since the motions of the vorticity anomalies are mainly driven by the horizontal flow, the advection term in Eq. (4) is analyzed to understand the inward motion of the negative vorticity anomalies as displayed in Fig. 14. The tendency of the perturbation vorticity induced by the horizontal advection can be rewritten as

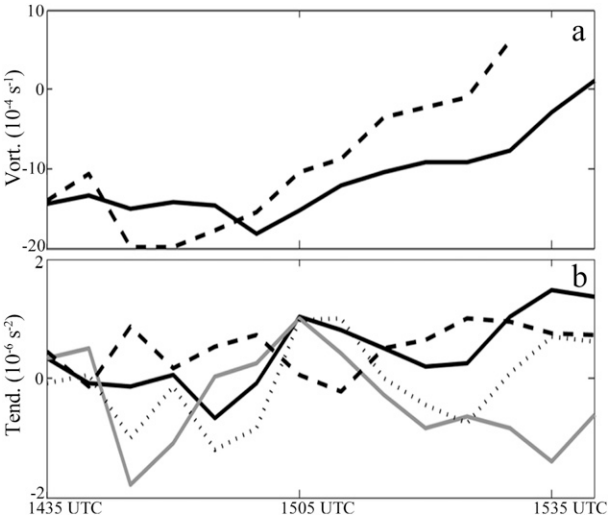

FIG. 15. (a) Time evolution of the maximum 188-m relative vorticity of the anomalies in the small boxes in Fig. 14. Solid and dashed lines denote the northern and southern anomalies, respectively. (b) Time evolution of the 188-m vorticity tendency (solid line) and that induced by the divergence of advective flux (dashed line) and nonadvective flux (dotted line) at the center of the northern negative vorticity anomaly. The gray curve in (b) denotes the horizontal divergence ($\times 10^{-4}$ s^{-1}).

$$\left.\frac{\partial \zeta'}{\partial t}\right|_{\text{adv}} = \underbrace{-\overline{u}\frac{\partial \zeta'}{\partial x} - \overline{v}\frac{\partial \zeta'}{\partial y}}_{1} \underbrace{-u'\frac{\partial \zeta'}{\partial x} - v'\frac{\partial \zeta'}{\partial y}}_{2} \underbrace{-u'\frac{\partial \overline{\zeta}}{\partial x} - v'\frac{\partial \overline{\zeta}}{\partial y}}_{3}, \tag{5}$$

where overbar denotes the background (axisymmetric) variables and the prime denotes the perturbation component. The change in the vorticity anomalies results from the advection of perturbation vorticity by the background and perturbation flows [terms 1 and 2 on the rhs of Eq. (5)] and the advection of the background vorticity by the perturbation flow [term 3 on rhs of Eq. (5)]. If a negative vorticity perturbation is imposed on an axisymmetric cyclonic vortex, the third term on the right-hand side of Eq. (5) will lead to a negative (positive) vorticity tendency on the left (right) side of the original perturbation facing the axisymmetric vortex center. Through the second term on the right-hand side of Eq. (5), the newly produced vorticity anomalies tend to drive the negative vorticity perturbation away from the axisymmetric vortex center. Therefore, the spiraling inward motion of the negative vorticity anomalies shown in Fig. 14 implies that the advection of the perturbation vorticity by the background inflow [term 1 on rhs of Eq. (5)] dominates over the interaction between vorticity anomalies [term 2 on rhs of Eq. (5)].

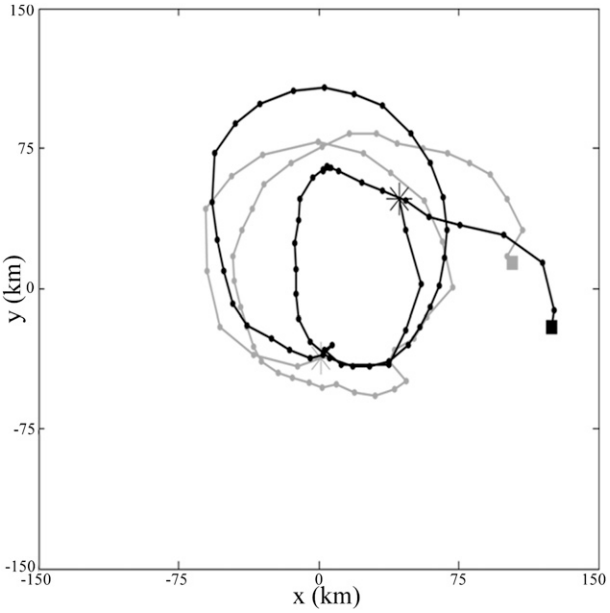

FIG. 16. Tracks of the CVA clusters C1 (black) and C2 (gray) denoted in Fig. 1. The squares and stars denote the start and end of each track, respectively. Interval along trajectories denoted by black and gray dots is 30 min.

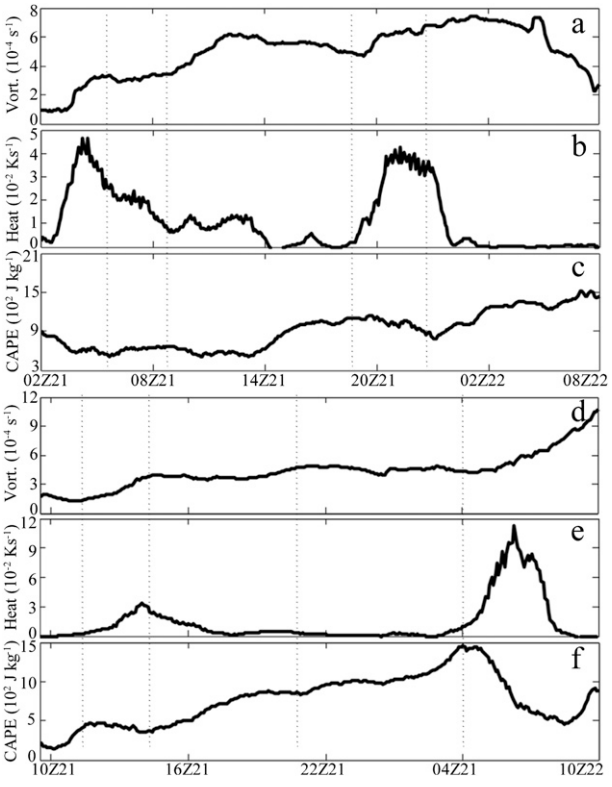

FIG. 17. Time evolution of (a) the 188-m relative vorticity, (b) 0–12-km averaged diabatic heating, and (c) surface-based CAPE averaged in the domain of 60 km × 60 km centered at the CVA cluster C1. (d)–(f) As in (a)–(c), but for the CVA cluster C2.

Compared to the cyclonic CVAs, the negative vorticity anomalies are usually weaker and shorter lived as they move toward the storm center. From Figs. 14 and 15a, we can see that the southern negative CVA almost disappears at 1529 UTC 22 July while the northern one reverses to be positive after around 1535 UTC 22 July. To understand the processes responsible for the weakening of the negative CVAs, the CVAs' vorticity tendency induced by the divergence of the advective flux [summation of the horizontal advection and stretching terms in Eq. (4)] and nonadvective flux [summation of the tilting and vertical advection terms in Eq. (4)] is calculated as suggested by Tory and Montgomery (2008). As an example, the vorticity tendency of the northern negative CVA in Fig. 14 is displayed in Fig. 15b. From this image, it is observed that the northern negative CVA begins to emerge within a convergent environment after around 1510 UTC 22 July. As a result, the positive vorticity associated with the cyclonic CVAs surrounding the negative CVA is converged into the area of the negative CVA, which, along with the friction and diffusion associated with the subgrid-scale processes, outweighs the negative vorticity tendency induced by the nonadvective flux terms and ultimately results in the decay of this negative CVA (Fig. 15b). Therefore, pertaining to Hurricane Dolly, there is no evidence that the storm's development is preceded by the expulsion of negative vorticity anomalies.

5. Cluster-scale processes occurring during the developing stage of hurricane Dolly

As a bridge between the system- and convective-scale components, the cluster-scale component exhibits features similar to those that occur on the other two scales. As an example, the evolution of CVA clusters C1 and C2 denoted in Fig. 1c are tracked. Figure 16 shows the tracks of C1 and C2. C1 originates near 0200 UTC 21 July and then circles around the storm center (Fig. 16). During this period, the mean relative vorticity of C1 varies closely with the mean CAPE and diabatic heating at the cluster scales (Figs. 17a–c). The significant increase in vorticity is usually accompanied by a decrease in CAPE and an increase in diabatic heating, while in the episode that the vorticity is nearly stationary or decreasing, the CAPE usually accumulates and the diabatic heating is simultaneously reduced. Such processes can also be identified in the evolution of CVA cluster C2 as shown in Figs. 17d–f. The similar relationships between patterns of vorticity and CAPE on the cluster and convective scales indicate that there are self-similarities that exist in the vortex at different scales.

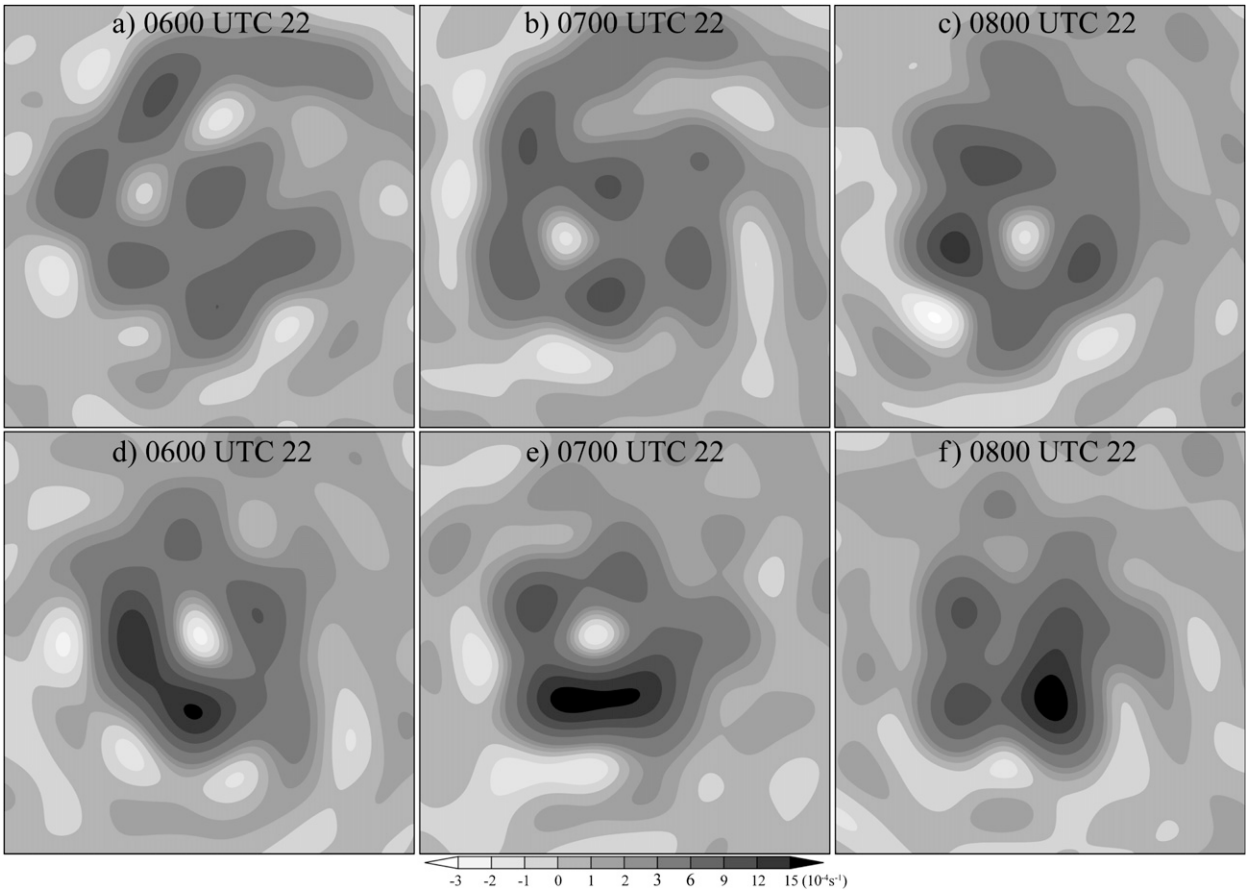

FIG. 18. The plan view of the vorticity anomalies with the scales larger than 50 km every 1 h from 0600 to 1100 UTC 22 July. The shading denotes the 188-m relative vorticity and the domain size is 240 km × 240 km.

Similar to what occurred on the convective scales, expulsions of negative vorticity anomalies are also not prevalent at the cluster and larger scales. Figure 18 displays the horizontal distribution of the relative vorticity summed from the cluster and system scales at different times during Dolly's development. It is clear that, instead of moving outward from the storm-centered area, the negative vorticity anomaly surrounded by the positive vorticity anomalies decays gradually and finally disappears.

6. Concluding remarks

Based on the descriptive analysis on the three-stage development process of Hurricane Dolly carried out in FZ10, this study further examines the evolution of, and interactions among, multiscale vortices ranging from the system-scale main vortex ($L > 150$ km) to the intermediate-scale cloud clusters (50 km $< L <$ 150 km), along with individual vorticity-rich convective cells ($L <$ 50 km). It is found that, during the developing stage of Dolly, the system-scale vortex enhances gradually within the framework of balanced dynamics while the convective-scale vortices are largely unbalanced and are nearly saturated soon after the initial burst of convection.

Based on the examination of the evolution of the vortices on different scales, the role of convection in the development of Dolly is further explored. On the convective scale, the convection induces instantaneous enhancement of the original CVAs or the formation of new CVAs, and, on the other hand, promotes the merger of CVAs via the accompanying convergent flow. In the system scale, the macroscopic effects of convection (i.e., diabatic heating) form a persistent thermal forcing and then result in a secondary circulation to implement the adjustment of the momentum fields to the forcing. The horizontal branch of the secondary circulation (i.e., the significant low-level inflow) aggregates the ambient vorticity, cluster-, and convective-scale CVAs into the storm center region, which facilitates the merger of the CVAs. Continuous projection and conversion of smaller-scale vorticity into the larger scales will eventually lead to the spinup of the system-scale vortex. These results are consistent

with those obtained by Nolan (2007) and Montgomery et al. (2006).

Inspection on the evolution of CVAs shows that the maximum cyclonic vorticity of the long-lived CVAs generally exhibits an obvious negative correlation with CAPE. Along with the burst of convection, CAPE is reduced while the vorticity of the CVAs increases consequently. Following the burst of convection and sharp intensification of the CVAs, the CVAs usually evolve into an adjusting episode, during which the maximum value of the CVAs' vorticity decreases considerably while the low-level potential temperature, mixing ratio, and CAPE increase gradually as a result of the air–sea interaction, and a new episode of convective bursts is brewing. Moreover, our sensitivity experiments further demonstrate that pure vortex mergers through horizontal advection and diffusion are not efficient in intensifying the vortex. To some extent, the merger of CVAs that occurred in the development of Dolly may be ascribed to the active moist convection, which can promote the merger of CVAs via the concomitant convergent flow and increase of the vorticity between the CVAs.

During the development of Dolly, the expulsion of the negative vorticity anomalies is not as evident as that suggested by previous idealized simulations. Instead, under the effect of system-scale convergent flow, the negative vorticity anomalies also move toward the central storm area. However, due to the considerable horizontal convergence of the cyclonic vorticity flux in the central storm area, the negative vorticity anomalies usually decay and then disappear en route toward the storm center.

Although the current work attempts to give a detailed description on the evolution of the CVAs and their relation to the convection in the TC development, it is necessary to concede that the analysis and results mentioned above are only based on a single case and a single numerical simulation of Hurricane Dolly spawned in the ''pouch'' of an easterly wave and may not work as well in the development of other hurricanes, such as those arising from monsoon troughs, the intertropical convergence zone (ITCZ), and so on. To obtain a comprehensive understanding of the CVAs, more effort is required to investigate more cases via high-resolution observational data and numerical simulations.

Acknowledgments. The research was conducted during the first author's sabbatical visit at Texas A&M University and The Pennsylvania State University. The authors are grateful for constructive comments by Bill Frank, Yonghui Weng, and Dave Nolan and for the proofreading by Thomas Hinson and Daniel Stern. This work was supported in part by Office of Naval Research Grant N000140910526, National Science Foundation Grants ATM-0840651 and ATM-063064, Nature Science Foundation of China Grants 40921160382 and 40830958, and the State Key Basic Program of China (2009CB421502).

REFERENCES

Black, M. L., R. W. Burpee, and F. D. Marks Jr., 1996: Vertical motion characteristics of tropical cyclones determined with airborne Doppler radial velocities. *J. Atmos. Sci.,* **53,** 1887–1909.

Bui, H., K. Smith, M. T. Montgomery, and J. Peng, 2009: Balanced and unbalanced aspects of tropical cyclone intensification. *Quart. J. Roy. Meteor. Soc.,* **135,** 1715–1731.

Charney, J. G., and A. Eliassen, 1964: On the growth of the hurricane depression. *J. Atmos. Sci.,* **21,** 68–75.

Chen, S. S., and W. M. Frank, 1993: A numerical study of the genesis of extratropical convective mesovortices. Part I: Evolution and dynamics. *J. Atmos. Sci.,* **50,** 2401–2426.

Davis, C. A., and K. A. Emanuel, 1991: Potential vorticity diagnostics of cyclogenesis. *Mon. Wea. Rev.,* **119,** 1929–1953.

——, and L. F. Bosart, 2006: The formation of Hurricane Humberto (2001): The importance of extra-tropical precursors. *Quart. J. Roy. Meteor. Soc.,* **132,** 2055–2085.

Dunkerton, T. J., M. T. Montgomery, and Z. Wang, 2008: Tropical cyclogenesis in a tropical wave critical layer: Easterly waves. *Atmos. Chem. Phys. Discuss.,* **8,** 11 149–11 292.

Emanuel, K. A., 1986: An air–sea interaction theory for tropical cyclones. Part I: Steady state maintenance. *J. Atmos. Sci.,* **43,** 585–604.

Fang, J., and F. Zhang, 2010: Initial development and genesis of Hurricane Dolly (2008). *J. Atmos. Sci.,* **67,** 655–672.

Frank, W. M., 1983: The cumulus parameterization problems. *Mon. Wea. Rev.,* **111,** 1859–1871.

Hack, J. J., and W. H. Schubert, 1986: Nonlinear response of atmospheric vortices to heating by organized cumulus convection. *J. Atmos. Sci.,* **43,** 1559–1573.

Hawblitzel, D. P., F. Zhang, Z. Meng, and C. A. Davis, 2007: Probabilistic evaluation of the dynamics and predictability of the mesoscale convective vortex of 10–13 June 2003. *Mon. Wea. Rev.,* **135,** 1544–1563.

Haynes, P. H., and M. E. McIntyre, 1987: On the evolution of vorticity and potential vorticity in the presence of diabatic heating and frictional or other forces. *J. Atmos. Sci.,* **44,** 828–841.

Hendricks, E. A., M. T. Montgomery, and C. A. Davis, 2004: The role of ''vortical'' hot towers in the formation of tropical cyclone Diana (1984). *J. Atmos. Sci.,* **61,** 1209–1232.

Houze, R. A., Jr., W. C. Lee, and M. M. Bell, 2009: Convective contribution to the genesis of Hurricane Ophelia (2005). *Mon. Wea. Rev.,* **137,** 2778–2800.

Laing, A., and J.-L. Evans, cited 2010: *Introduction to Tropical Meteorology*. COMET. [Available online at http://www.meted.ucar.edu/tropical/textbook.]

Lin, Y., and F. Zhang, 2008: Tracing mesoscale gravity waves in baroclinic jet-front systems. *J. Atmos. Sci.,* **65,** 2402–2415.

Marks, F. D., and R. A. Houze Jr., 1984: Airborne Doppler radar observations in Hurricane Debby. *Bull. Amer. Meteor. Soc.,* **65,** 569–582.

——, P. G. Black, M. T. Montgomery, and R. W. Burpee, 2008: Structure of the eye and eyewall of Hurricane Hugo (1989). *Mon. Wea. Rev.,* **136,** 1237–1259.

McWilliams, J. C., 1985: A uniformly valid model spanning the regimes of geostrophic and isotropic, stratified turbulence: Balanced turbulence. *J. Atmos. Sci.,* **42,** 1773–1774.

Montgomery, M. T., and J. Enagonio, 1998: Tropical cyclogenesis via convectively forced vortex Rossby waves in a three-dimensional quasigeostrophic model. *J. Atmos. Sci.,* **55,** 3176–3207.

——, M. E. Nicholls, T. A. Cram, and A. B. Saunders, 2006: A vortical hot tower route to tropical cyclogenesis. *J. Atmos. Sci.,* **63,** 355–386.

——, S. V. Nguyen, R. K. Smith, and J. Persing, 2009: Do tropical cyclones intensify by WISHE? *Quart. J. Roy. Meteor. Soc.,* **135,** 1697–1714.

Nguyen, S. V., R. K. Smith, and M. T. Montgomery, 2008: Tropical-cyclone intensification and predictability in three dimensions. *Quart. J. Roy. Meteor. Soc.,* **134,** 563–582.

Nolan, D. S., 2007: What is the trigger for tropical cyclogenesis? *Aust. Meteor. Mag.,* **56,** 241–266.

——, and L. D. Grasso, 2003: Three-dimensional, nonhydrostatic perturbations to balanced, hurricane-like vortices. Part II: Symmetric response and nonlinear simulations. *J. Atmos. Sci.,* **60,** 2717–2745.

——, M. T. Montgomery, and L. D. Grasso, 2001: The wavenumber one instability and trochoidal motion of hurricane-like vortices. *J. Atmos. Sci.,* **58,** 3243–3270.

——, Y. Moon, and D. P. Stern, 2007: Tropical cyclone intensification from asymmetric convection: Energetics and efficiency. *J. Atmos. Sci.,* **64,** 3377–3405.

Ooyama, K., 1964: A dynamical model for the study of tropical cyclone development. *Geofis. Int.,* **4,** 187–198.

——, 1982: Conceptual evolution of the theory and modeling of the tropical cyclone. *J. Meteor. Soc. Japan,* **60,** 369–370.

Pendergrass, A. G., and H. E. Willoughby, 2009: Diabatically induced secondary flows in tropical cyclones. Part I: Quasi-steady forcing. *Mon. Wea. Rev.,* **137,** 805–821.

Press, W. H., S. A. Teukolsky, W. T. Vetterling, and B. P. Flannery, 1992: *Numerical Recipes in FORTRAN 77: The Art of Scientific Computing*. Vol. 1. 2nd ed. Cambridge University Press, 933 pp.

Raymond, D. J., and H. Jiang, 1990: A theory for long-lived mesoscale convective systems. *J. Atmos. Sci.,* **47,** 3067–3077.

Reasor, P. D., M. T. Montgomery, and L. F. Bosart, 2005: Mesoscale observations in the genesis of Hurricane Dolly (1996). *J. Atmos. Sci.,* **62,** 3151–3171.

Rogers, R. F., M. L. Black, S. S. Chen, and R. A. Black, 2007: An evaluation of microphysics fields from mesoscale model simulation of tropical cyclones. Part I: Comparisons with observations. *J. Atmos. Sci.,* **64,** 1811–1834.

Rotunno, R., and K. A. Emanuel, 1987: An air–sea interaction theory for tropical cyclones. Part II: Evolutionary study using a nonhydrostatic axisymmetric numerical model. *J. Atmos. Sci.,* **44,** 542–561.

Schubert, W. H., and J. J. Hack, 1982: Inertial stability and tropical cyclone development. *J. Atmos. Sci.,* **39,** 1687–1697.

——, ——, P. L. Silva Dias, and S. R. Fulton, 1980: Geostrophic adjustment in an axisymmetric vortex. *J. Atmos. Sci.,* **37,** 1464–1484.

Shapiro, L. J., and H. Willoughby, 1982: The response of balanced hurricanes to local sources of heat and momentum. *J. Atmos. Sci.,* **39,** 378–394.

Sippel, J. A., J. W. Nielsen-Gammon, and S. E. Allen, 2006: The multiple-vortex nature of tropical cyclogenesis. *Mon. Wea. Rev.,* **134,** 1796–1814.

Tory, K. J., and M. T. Montgomery, 2008: Tropical cyclone formation: A synopsis of the internal dynamics. Preprints, *28th Conf. on Hurricanes and Tropical Meteorology,* Orlando FL, Amer. Meteor. Soc., 10A.1. [Available online at http://ams.confex.com/ams/pdfpapers/138062.pdf.]

——, ——, and N. E. Davidson, 2006a: Prediction and diagnosis of tropical cyclone formation in an NWP system. Part I: The critical role of vortex enhancement in deep convection. *J. Atmos. Sci.,* **63,** 3077–3089.

——, ——, ——, and J. D. Kepert, 2006b: Prediction and diagnosis of tropical cyclone formation in an NWP system. Part II: A diagnosis of Tropical Cyclone Chris formation. *J. Atmos. Sci.,* **63,** 3091–3113.

Willoughby, H., 1990: Gradient balance in tropical cyclones. *J. Atmos. Sci.,* **47,** 265–274.

——, 2009: Diabatically induced secondary flows in tropical cyclones. Part II: Periodic forcing. *Mon. Wea. Rev.,* **137,** 822–835.

Wu, L., and S. A. Braun, 2004: Effects of environmentally induced asymmetries on hurricane intensity: A numerical study. *J. Atmos. Sci.,* **61,** 3065–3081.

Yuter, S. E., and R. A. Houze Jr., 1995: Three-dimensional kinematic and microphysical evolution of Florida cumulonimbus. Part III: Vertical mass transport, mass divergence, and synthesis. *Mon. Wea. Rev.,* **123,** 1964–1983.

Zhang, D.-L., and C. Q. Kieu, 2005: Shear-forced vertical circulations in tropical cyclones. *Geophys. Res. Lett.,* **32,** L13822, doi:10.1029/2005GL023146.

Zhang, F., and J. A. Sippel, 2009: Effects of moist convection on hurricane predictability. *J. Atmos. Sci.,* **66,** 1944–1961.